MONTE CARLO SIMULATION OF TREE CANOPY SCATTERING AND PROPAGATION

Thesis

Submitted to

The School of Engineering of the

UNIVERSITY OF DAYTON

in Partial Fulfillment of the Requirements for

The Degree

Master of Science in Electro-Optics

by

Michael A. Greiner

UNIVERSITY OF DAYTON

Dayton, Ohio

May, 2007

MONTE CARLO SIMULATION OF TREE CANOPY SCATTERING AND PROPAGATION

APPROVED BY:

Bradley A. Duncan, PhD.
Professor,
Electro-Optics Program
University of Dayton
Committee Chairman

Matthew P. Dierking
Principal Scientist
Sensors Directorate
Air Force Research Lab
Committee Member

Joseph W. Haus, PhD.
Director and Professor,
Electro-Optics Program
University of Dayton
Committee Member

Donald L. Moon, Ph.D.
Associate Dean
Graduate Engineering Programs
& Research
School of Engineering

Joseph E. Saliba, Ph.D., P.E.
Dean
School of Engineering

Abstract

MONTE CARLO SIMULATION OF TREE CANOPY SCATTERING AND PROPAGATION

Michael A. Greiner
University of Dayton

Advisor: Dr. Bradley D. Duncan

The objective of this research is to investigate the physical and optical properties of tree canopies in order to develop an improved foliage penetration model. This project can be broken into two separate segments: experimental and simulation. The experimental portion presents our investigations into the optical scattering properties of both maple and cottonwood leaves in the near-infrared wavelength regime. The bidirectional scattering distribution function (BSDF) describes the fractions of light reflected by and transmitted through a leaf for a given set of illumination and observation angles. Experiments were performed to measure the BSDF of each species at a discrete set of illumination and observation angles. We then modeled the BSDF's in such a way that other researchers may interpolate their values for scattering in any direction under illumination at any angle.

In the modeling segment of the research we created a Monte Carlo algorithm for tracking the propagation of photons through a canopy consisting of many randomly distributed leaves. We used several different methods for modeling the individual scatterers based on the experimental results: ideal Lambertian, Lambertian-Rayleigh, and

the interpolated data model. The output coordinates of the photons were saved and used quantify the temporal, spatial, and angular dispersion experienced by an incident pencil beam through a foliated forest canopy. The results of each leaf model were then compared such that an optimum method was determined.

Acknowledgements

This effort was supported in part by the U.S. Air Force and Anteon, Inc., of Dayton, OH through contract number F33601-02-F-A581, and by the Ladar and Optical Communications Institute (LOCI) at the University of Dayton.

The authors wish to thank John Schmoll, Larry Barnes, Tim Meade and Dave Mohler, of AFRL/SNJM, for their invaluable guidance and assistance.

The views expressed in this article are those of the authors and do not reflect on the official policy of the Air Force, Department of Defense or the U.S. Government.

Table of Contents

List of Illustrations

List of Tables

Chapter 1

Introduction

1.1Background

Forested areas are important from a remote sensing standpoint as they cover large parts of the earth. Because more than 23% of the earth's surface is still covered by forest, the interaction of light and matter above, within, and below the forest canopy is of interest.[1] The ability to model the propagation of light through these forested areas is important for a number of environmental uses, such as monitoring the earth's resources, topographic mapping of the land surface beneath jungle or forest terrain, and increasing agricultural efficiency.[2,3] In addition, foliage penetration models are used in the field of remote sensing. Detecting objects beneath jungle and forest canopies is a difficulty for current remote sensing procedures.[4] These applications, along with a lack of suitable foliage penetration techniques drive a pressing need for an accurate canopy propagation model.

1.2Problem Statement

Current foliage penetration methods depend heavily on looking between gaps in the leaves and branches to see what lies below.[4] Unfortunately, as the foliage density or zenith angle increases the gap fraction quickly drops to zero, leaving very few

opportunities to find gaps in the canopy, as can be seen in Figure 1.1 below. The ability to look directly through the leaves and not rely on the gaps between the leaves will greatly aid the imaging of objects beneath the canopy.

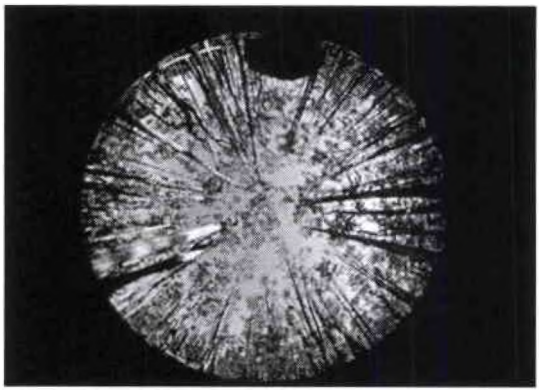

Figure 1.1 Gap fraction of a canopy seen looking upward through a fisheye lens[6]

There exist many models of canopy propagation which attempt to replicate the scattering of light through a canopy of leaves.[7,8,9] However, most current foliage penetration models assume leaves to be perfect Lambertian scatterers. Where this is generally a reasonable assumption, it neglects to consider the specular reflection component of leaves as the illumination angle gets large.[10,11] Ignoring the high angle specular reflection of leaves affects the angular distribution of light emerging from the canopy and consequently the interpretation of the resulting data.

1.3Research Objective

The objective of this research is to investigate the physical and optical properties of canopies in order to develop an improved foliage penetration model. This project can be broken into two separate segments: experimental and simulation. The goal of the experimental portion of the research is to quantify and characterize the optical properties

of leaves for 1.06 μm laser light. The results from the experimental portion are then used in the modeling portion to simulate the exchange of energy between an incident laser beam and a canopy. The goal of the modeling portion of the research is to quantify the temporal, spatial, and angular dispersion experienced by an incident pencil beam through a foliated forest canopy.

1.4Methodology

The optical properties of leaves are characterized using a goniometrical apparatus which allows the measurement of the optical scattering profile for species of leaves at variable illumination angles. The function describing the reflectance, transmittance, and absorptance properties of the leaves as a function of both incident and observation angles is known as the bidirectional scattering distribution function (BSDF). The BSDFs are measured for local maple and cottonwood leaves at a wavelength of 1.06 μm. The data is then fitted to a model such that the BSDF for any set of illumination and observation angles can be interpolated.

A Monte Carlo simulation of the propagation of photons through a random canopy is created using several BSDF models along with other parameters describing the physical characteristics of the canopy. The spatial, angular, and temporal statistics of millions of normally incident photons are calculated and stored for the photons as they exit the canopy. The paths of the exiting photons are traced through free space to the plane of an imaging detector 50 meters above the canopy. Finally, spatio-temporal plots of the arrival times and locations of the photons onto the imaging detector are compared for each BSDF model.

Chapter 2

Background Theory

Because of the dependence of the modeling on some key statistical models, it is important to define some of the tools used in this research. The following sections provide a brief overview of the statistical concepts necessary for creating a model of the system at hand.

2.1Random Variables

In a random experiment the collection of observed results is governed by the probability that each possible event will occur. The probability that a specific event E will occur is defined to be the ratio of the number of observed instances of that event, n_E, to the total number of trials in the experiment, N, as expressed in Equation 2.1.

$$P\{E\} = \frac{n_E}{N} \tag{2.1}$$

A random variable U is a process, rule or a function which assigns a numerical value $u(w)$ to every possible event w in a random experiment. Using a random variable it is possible to map all possible outcomes of a random experiment to the real number line. One can associate a probability with the relative frequency with which a random variable takes on a particular value. Description of random variables using probability is

done primarily in two ways. The two methods of describing random variables using probability that are of particular interest are the cumulative distribution function (cdf) and the probability density function (pdf).

2.1.1 Cumulative Distribution and Probability Density Functions

The cumulative distribution function of a random variable is defined to be the probability that the random variable X takes on a value that is less than or equal to a possible numerical outcome x. The cdf of a random variable can be mathematically expressed as

$$F_X(x) = P\{X \leq x\}. \tag{2.2}$$

An example of a typical cdf can be seen in Figure 2.1.

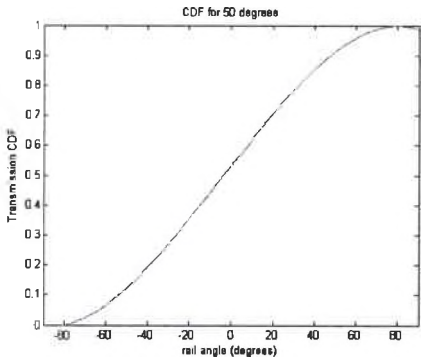

Figure 2.1 Typical curve of a Cumulative Distribution Function

From the shape of the curve in Figure 2.1, it is possible to infer some general properties of cdf's:

i. The limiting values of the cdf are given by

$$F_X(-\infty) = 0 \text{ and } F_X(\infty) = 1$$

ii. $F_X(x)$ is always non-decreasing.

iii. The probability that the random variable is greater than the outcome x is given by,

$$P\{X > x\} = 1 - F_X(x).$$

The probability that the random variable is between x_1 and x_2 is given by,

$$P\{x_1 \leq X \leq x_2\} = F_X(x_2) - F_X(x_1) \tag{2.3}$$

Another important method of describing a random variable using probabilities is the probability density function. The pdf of a random variable is defined to be the derivative of the cdf, expressed as

$$p_X(x) = \frac{dF_X(x)}{dx}. \tag{2.4}$$

Where the cdf has units of probability, the pdf represents the probability per interval of the random variable X. Therefore, the probability that a random variable will lie within the infinitesimally small region $[x, x+dx]$ is given by

$$P\{x \leq X \leq x+dx\} = p_X(x)dx \tag{2.5}$$

So, the actual probability that a random variable will take on a value between x_1 and x_2 is found by integrating the pdf over the interval $[x_1, x_2]$. An example of a typical pdf can be seen in Figure 2.2. From the shape of the curve in Figure 2.2, one can infer some general properties of pdf's:

i. The limiting values of the pdf are given by

$$p_X(-\infty) = 0 \text{ and } p_X(\infty) = 0$$

ii. $p_X(x)$ is always non-negative.

iii. The integral of the pdf over all possible values is unity.

$$\int_{-\infty}^{\infty} p_X(x)dx = 1$$

iv. The integral of the pdf from $-\infty$ to u is the cdf:

$$\int_{-\infty}^{u} p_X(x)dx = F_X(x)$$

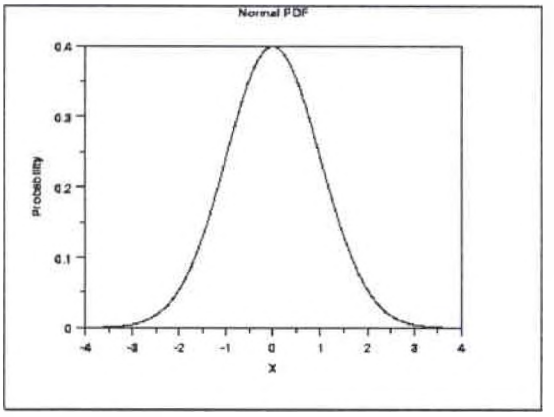

Figure 2.2 Typical curve of a Probability Density Function

2.1.2 Multi-Dimensional pdfs

Often times it is the case that there exists a multi-dimensional system consisting of multiple random variables X and Y, which each have their own individual statistics. One can describe the joint probability that both X and Y will take on certain values using the same functions as were used in the case of a single random variable. The joint distribution function, expressed as

$$F_{X,Y}(x, y) = P\{X \leq x, Y \leq y\}, \tag{2.6}$$

describes the probability that both X and Y will be less than or equal to x and y, respectively. Similarly, a joint probability density function can be created from the second partial derivative of the join distribution function, given by

$$p_{X,Y}(x,y) = \frac{d^2}{dxdy} F_{X,Y}(x,y). \tag{2.7}$$

As is the case with single variable pdf's, the joint pdf represents the probability that both X and Y will lie within infinitesimally small regions, expressed as

$$p_{X,Y}(x,y) = P\{x \le X \le x+dx, y \le Y \le y+dy\}. \tag{2.8}$$

The properties of the joint probability density function are much like those of the single variable pdf:

i. The joint pdf is always non-negative.

ii. The integral of the joint pdf over all possible values is unity.

$$\int_{-\infty}^{\infty}\int_{-\infty}^{\infty} p_{X,Y}(x,y)dxdy = 1 \tag{2.9}$$

2.1.3 Statistically Independent pdfs

It is sometimes the case that the probability of one variable does not in any way depend on the probability of the other variable. In such instances, the two random variables are said to be statistically independent. For statistically independent random varaibles, the joint pdf of the two variables can be broken into the product of the individual, independent, single-variable pdfs of the two random variables.

$$p_{X,Y}(x,y) = p_X(x)p_Y(y) \tag{2.10}$$

2.1.4 Forward Transformations of Random Variables

Random variables are often times created by a function of another random variable. In general, consider the random variable Y which can be described as a function of the random variable X :

$$Y = f(X). \tag{2.11}$$

In the forward transformation of $p_X(x)$, the properties of X are known and the goal is to determine $p_Y(y)$ given $f(X)$ and $p_X(x)$. This is an important process, as many computer programs have uniformly distributed random number generators, and often times it is desired to select a random number governed by a different set of statistics.

For the moment, restrict f to be monotonic so that there is a 1:1 mapping between x and y. Figure 2.3 displays a general function f mapping the random variable x to y.

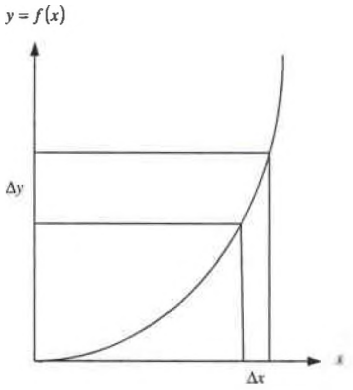

Figure 2.3 The mapping of one random variable, y, to another, x.

Notice, because there is a 1:1 mapping between the two variables, the probability of X being in the interval $[x, x+\Delta x]$ is the same as the probability of Y being in the interval $[y, y+\Delta y]$. Even though the size of the two regions being compared is not the same, the mathematical probability of picking a random number within either region is equal. Mathematically this is expressed,

$$P\{y \le Y \le y+\Delta y\} = P\{x \le X \le x+\Delta x\}. \tag{2.12}$$

Recall Equation 2.5, which states that the probability that a random variable will lie within the infinitesimally small region $[x, x+dx]$ has probability $p_X(x)dx$. Therefore, the above relation can be expressed

$$p_Y(y)dy = p_X(x)dx. \tag{2.13}$$

Solve for $p_Y(y)$ to yield,

$$p_Y(y) = p_X(x)\frac{dx}{dy}. \tag{2.14}$$

In the expression above, $p_Y(y)$ is in terms of x. The goal is to get $p_Y(y)$ in terms of y. The substitution $x = f^{-1}(y)$ is used to obtain a function of y, expressed

$$p_Y(y) = p_X(f^{-1}(y))\left|\frac{df^{-1}(y)}{dy}\right|. \tag{2.15}$$

As long as $f(x)$ is monotonic and there is a 1:1 correspondence between x and y the inverse function of f exists. For functions that are not monotonic, as seen in Figure 2.4, break $f(x)$ into regions that are monotonic, perform the transformation over each region, and simply add the results. Using Equation 2.15, it is possible to generate the statistics of any random variable given the functional relationship and pdf of a known random variable.

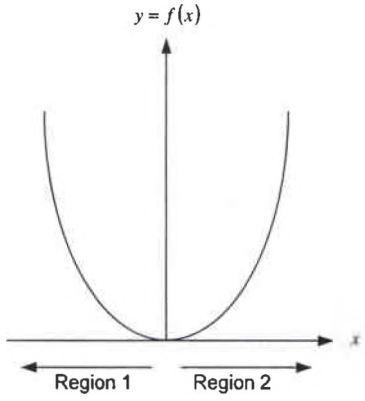

Figure 2.4 A non-monotonic function must be broken into sections where 1:1 correspondence is maintained.

2.1.5 Reverse Transformations of Random Variables

In general, random number generators will generate random numbers that are uniformly distributed over the interval $[0,1]$. Some programs can generate random numbers with other distributions. Where it is helpful to have various random number generators, only one is required. As seen in section 2.1.4, given any random variable and its probability density function, one can derive an expression for the pdf of another random variable related to the first by some transformation function. Using these results, it is also possible to perform a reverse transform a random variable X, where one can find the transformation function $f(X)$ given knowledge of the pdfs $p_X(x)$ and $p_Y(y)$.

Let X be uniformly distributed on the interval $[0,1]$ and let $f(X)$ be monotonic. Then, by Equation 2.15,

$$p_Y(y) = p_X\left(f^{-1}(y)\right)\left|\frac{df^{-1}(y)}{dy}\right|.$$

The probability density function of X has a value of 1 over the interval $[0,1]$ and is 0 otherwise. So the expression becomes

$$p_Y(y) = \begin{cases} \left|\dfrac{df^{-1}(y)}{dy}\right|, & 0 \le x \le 1 \\ 0 & \text{otherwise} \end{cases}. \tag{2.16}$$

The absolute value of a function is given to be the value of the function if the function is positive and minus the value of the function if the function is negative. The above expression can then be written,

$$p_Y(y)=\begin{cases}\dfrac{df^{-1}(y)}{dy}, & \text{derivative}\geq 0\\ -\dfrac{df^{-1}(y)}{dy}, & \text{derivative}<0\end{cases}. \tag{2.17}$$

Now, integrate and solve for $f^{-1}(y)=x$.

$$f^{-1}(y)=x=\begin{cases}\int_{-\infty}^{y} p_Y(y')dy', & \dfrac{df^{-1}(y)}{dy}\geq 0\\ -\int_{-\infty}^{y} p_Y(y')dy', & \dfrac{df^{-1}(y)}{dy}<0\end{cases} \tag{2.18}$$

Recall that the integral of the probability density function from $-\infty$ to y is the definition of the cumulative distribution function. Finally, the expression relating the two random variables is found to be

$$f^{-1}(y)=x=\begin{cases}F_Y(y), & \dfrac{df^{-1}(y)}{dy}\geq 0\\ -F_Y(y), & \dfrac{df^{-1}(y)}{dy}<0\end{cases}. \tag{2.19}$$

Recall that the cdf is always non-decreasing. Therefore, its derivative will always be greater than or equal to zero. Thus,

$$Y=f(X)=F_Y^{-1}(y). \tag{2.20}$$

Given a uniformly distributed random variable X, it is possible to generate a random variable Y such that the statistics of Y follow a desired probability distribution. Consider, for example, the transformation of a uniform random variable X to another random variable Y that has a pdf given by

$$p_Y(y)=\cos(y)\left[u(y)-u\left(y-\frac{\pi}{2}\right)\right]. \tag{2.21}$$

Integration of this pdf yields the result

$$F_Y(y) = \sin(y) = f^{-1}(y) = x. \tag{2.22}$$

The relationship between X and Y found in 2.22 gives X as a function of Y. Taking the inverse gives Y in terms of X, as is desired:

$$Y = \operatorname{asin}(X) \tag{2.23}$$

Note that as X varies between $[0,1]$, Y takes on values between $\left[0, \frac{\pi}{2}\right]$. These results will prove to be important later as many angular pdfs inherent to canopies take on cosine distributions.

2.2 *Monte Carlo Simulation*

The Monte Carlo method is a method for solving complex physical and mathematical problems using non-deterministic techniques. Monte Carlo methods make use of random number generation and statistical probability to solve very complex systems. Use of these methods allows one to solve problems that otherwise would not be solvable. For example, a system consisting of two particles and their interactions is fairly simple to solve analytically. Equations can be derived relating one particle's motion to the other. However, a system of hundreds of particles interacting with each other is impossible to solve analytically. There is no feasible way to derive the equations that would relate the motion and position of all the particles with respect to each other. Such a task is more easily solvable using Monte Carlo methods.

A Monte Carlo simulation entails generating a large number of random realizations of the system and calculating the statistics of the outcomes of the realizations.

The key concept behind this method is the law of large numbers, which states that the average of a large sample of a population will tend to the actual mean value of the population as the sample size increases towards infinity. A sample of the application of the Monte Carlo method is found in Appendix 1, where an approximation of pi is performed by randomly "throwing darts" at a circular dart board.

2.3 Photon Scattering

When a photon interacts with a material, three types of interactions may occur: reflection, transmittance and absorption. Absorbed photons are converted into energy by the material, usually in the form of heat. Reflected and transmitted photons are scattered from the material in a random direction based on surface and sub-surface interactions with the material structure.

Snell's law of reflection which states that the angle of incidence that light makes with a surface is equal to the angle of reflection of light from that surface. This law is true for smooth surfaces such as mirrors. However, many times scattering is not as simple as the reflection of light from a mirror. When light strikes a microscopically rough or granular surface, it bounces off in all directions due to the irregularities of the interface, as illustrated in Figure 2.5. So the reflection of light from such a surface should be thought of more as a re-distribution of light in all directions. The exact form of this diffuse reflection depends on the structure of the surface.

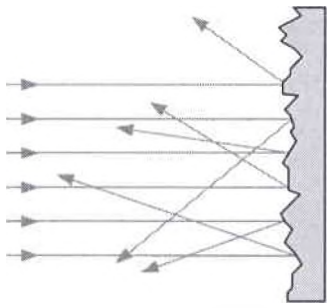

Figure 2.5 Scattering from a rough surface distributes light in all directions

Similarly, Snell's Law of refraction allows one to calculate the angle of transmission of a light beam upon striking a material.

$$n_1 \sin\theta_1 = n_2 \sin\theta_2 \tag{2.24}$$

Snell's Law, given in Equation 2.26, is analogous to the idealized case of mirror-like reflection of light from a surface. Light is transmitted in only one direction based on the ratio of the indices of refraction of the two interacting media. However, just as not all reflected photons leave a rough surface in the same direction, not all the transmitted photons leave a diffusing medium in the same direction. The microscopic irregularities within a diffusely scatterign body also scatter the transmitted light in many directions. The exact form of transmission also depends on the structure of the material.

2.3.1 Bidirectional Scattering Distribution Functions

The characterization of the scattering profile of light from a surface is known as the bidirectional scattering distribution function. The BSDF characterizes how much light is scattered (reflected and transmitted) from a surface in each direction. The BSDF is typically split into the reflected and transmitted components, which are treated separately as the bidirectional reflectance distribution function (BRDF) and the bidirectional transmittance distribution function (BTDF).

In general, the amount of light that is scattered depends on the direction of the incident light with respect to the surface normal and the angle at which the viewer observes the reflection. As a consequence, the function is dependent upon two directional angles: the angle of illumination and the angle at which light is being scattered. Also note that both the BRDF and the BTDF consist of two separate components, diffuse and specular., as seen in Figure 2.6

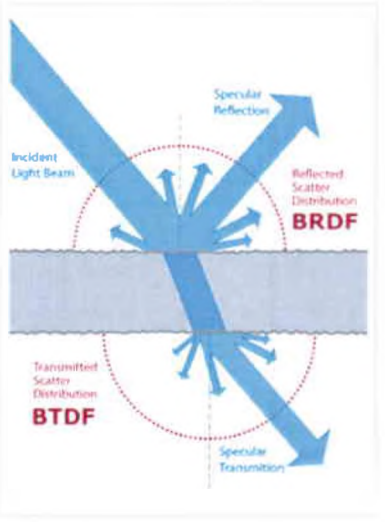

Figure 2.6 Bidirectional Scattering Distribution Function can be split into the BRDF and the BTDF, each of which is composed of a diffuse and specular component.[42]

A very common, naturally occurring BSDF is the Lambertian distribution. Lambert's cosine law says that the intensity observed from a Lambertian scatterer is directly proportional to the cosine of the angle made between the observer and the surface normal. That is, the observed intensity is a maximum at the surface normal and drops as a function of cosine as the observation angle changes from normal. Regardless of the illumination angle, the BSDF of a Lambertian scatterer varies as the cosine of the observation angle. Some examples of naturally occurring Lambertian scatteres include dirt and snow.

2.3.2 Reflection, Transmission, and Absorption Coefficients

The scattering and absorption profiles of matter can be characterized by the reflection, transmission, and absorption coefficients: R, T, and A. The reflection coefficient R is defined to be the ratio of the power reflected from a surface to the total power incident upon that surface. Similarly, the transmission coefficient T is defined to be the ratio of the transmitted power to the total power and the absorption coefficient A is defined as the ratio of the absorbed power to the total power. The sum of the three coefficients is unity, as there are only three options for a ray of light incident upon an interface.

$$R+T+A=1 \tag{2.25}$$

The BRDF is the ratio of the radiance reflected into a viewing direction and the incoming irradiance from one direction.[34] That is, if the total irradiance illuminating a material from a set of given incident angles (θ_I,ϕ_I) is I_0, and the amount of irradiance measured at a set observation angles (θ_D,ϕ_D) is given by $I(\theta_D,\phi_D)$, then the value for the BRDF for these given angles can be expressed as

$$\mathrm{BRDF}_\lambda(\theta_I,\phi_I,\theta_D,\phi_D)=\frac{I(\theta_D,\phi_D)}{I_0}. \tag{2.26}$$

Therefore, the sum of the BRDF over all observation angles is equal to the ratio of the total reflected radiance to the total incident irradiance.

$$\iint \mathrm{BRDF}_\lambda(\theta_I,\phi_I,\theta_D,\phi_D)\,d\theta_D d\phi_D = \iint \frac{I(\theta_D,\phi_D)}{I_0} d\theta_D d\phi_D = \frac{I_R}{I_0} = R \tag{2.27}$$

Note this ratio is also defined to be the reflection coefficient. Similarly, the sum of the BTDF over all observation angles is equal to the transmission coefficient.

$$\iint \mathrm{BTDF}_{\lambda}(\theta_I, \phi_I, \theta_D, \phi_D)\, d\theta_D d\phi_D = \frac{I_T}{I_0} = T \tag{2.28}$$

The absorption coefficient can then be calculated by using Equation 2.25 and substituting in the found values for R and T.

Chapter 3

BSDF Measurements

The scattering and transmission properties of trees and forests are topics of great interest in the field of optical remote sensing. As leaves dominate the scattering of light within a forest canopy, knowledge of their optical properties is essential in order to model the interaction of photons with the canopy. Optical properties of leaves have been the subject of many studies in recent years. These studies have found applications in several fields, including photobiology, agriculture and remote sensing.[1,2,3]

This article focuses upon the bidirectional scattering distribution function (BSDF) of maple and cottonwood leaves. The BSDF of a surface is the ratio of the scattered radiance to incident irradiance at a given wavelength. The function is dependent upon two directional angles, the angle of illumination and the angle at which light is scattered. The BSDF is typically split into reflected and transmitted components, which are treated separately as the bidirectional reflectance distribution function (BRDF) and the bidirectional transmittance distribution function (BTDF), respectively.

Few studies have been performed on the scattering functions of individual leaves because it has typically been assumed that these functions are simply Lambertian in nature.[4, 5] However, measurements have not always supported this assumption. In fact,

some studies, including our own, have found a strong specular reflection component accompanying the diffuse Lambertian scattering for higher illumination angles.[6,7,8]

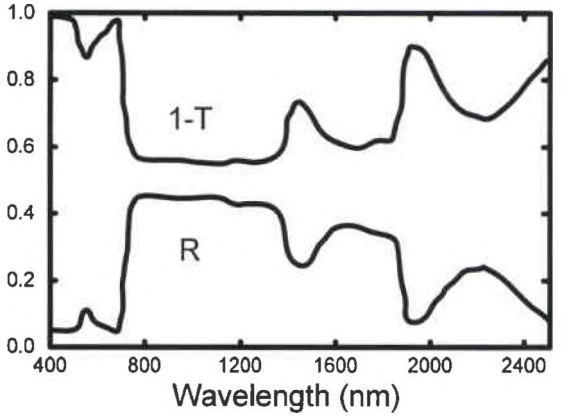

Figure 3.1 Reflectance and transmittance spectra of fresh poplar leaves.[9]

It has been demonstrated that the wavelength of the illuminating laser dramatically changes the scattering properties of leaves. Figure 3.1, for example, depicts the reflectance and transmittance spectra of fresh poplar leaves.[9] Although poplar is not one of the species investigated in this research, the general trend in its absorption spectrum is typical of all deciduous leaves and is therefore relevant to our work. Figure 1 is broken into three distinct regions: transmittance T, reflectance R, and absorptance A, where the absorptance is determined from T and R through the relationship $A = 1 - R - T$. Notice that the visible region is characterized by high absorptance. There are also strong absorption peaks in the infrared. However, there is a region in the near-IR, between 800 and 1300 nm, where absorptance is minimized. Selecting a wavelength in this region therefore provides the largest amount of light reflected by and transmitted through the leaves. It will thus be the goal of this research to characterize the BSDF's of two deciduous leaf species in the local Dayton, OH area (i.e., common maple and cottonwood) at a single, near-IR wavelength.

3.1 Experimental Setup

Measurement of BSDF data from individual leaves is performed through the use of the goniometric apparatus shown in Figure 3.2 and depicted schematically in Figure 3.3. A linearly polarized 1064 nanometer pulsed laser (>6μJ pulse energy) is directed along the axis of a stationary optical rail. A beam splitter is used to send half of the beam to the leaf for scattering and the other half to an energy level detector. The beam directed towards the energy detector is first incident upon a 50% reflective Spectralon® disc. The measured radiant energy reflected from this disc is simply used to monitor pulse-to-pulse energy fluctuations so that data can later be normalized with respect to variations in pulse energy.

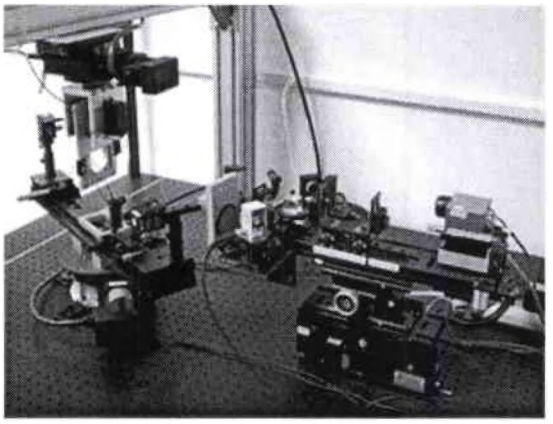

Figure 3.2 Photograph of the BSDF measurement apparatus

Two neutral density filters, mounted on the rail after the beam splitter, are used to attenuate the power of the laser in order to avoid damaging the transmission and reflection detectors. The ND filters are also tilted slightly in order to avoid direct reflections into the beam path. Notice, though, that any deflection of the beam due to the first filter is counteracted by the second so that the path of the beam remains along the rail axis.

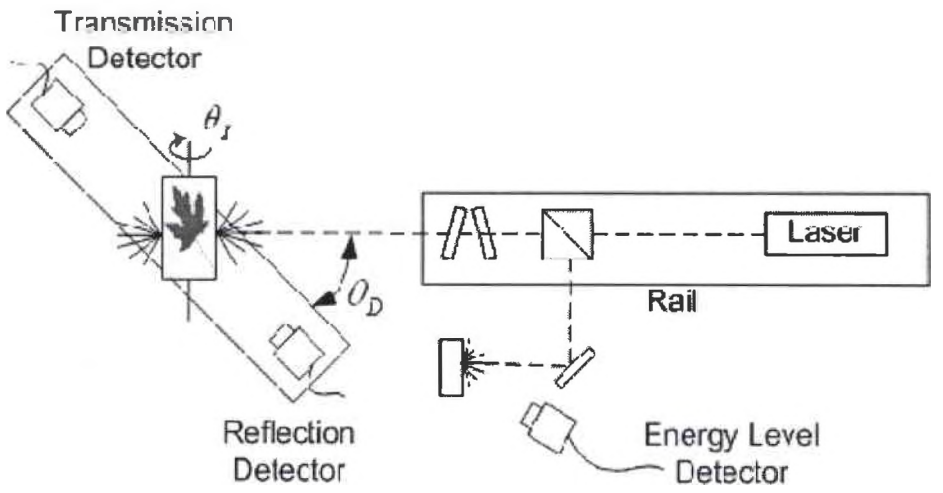

Figure 3.3 Schematic diagram of the BSDF measurement apparatus

After attenuation, the laser beam is directed onto the leaf, which is mounted in a goniometer for measurement. The goniometer has two separate, coaxial rotation stages that are motor driven and independently controlled by a computer which also tracks the leaf's rotational position relative to the beam path. A second optical rail is mounted on one of the rotation stages with reflection and transmission detectors equidistant from the leaf at opposite ends of the rail. The active region of the detectors is small enough to give point measurements and avoid angular averaging of the data. The leaf is mounted above this rail on a second rotation stage which is driven by a separate motor. In this way the illumination angle of the beam on the leaf can be adjusted independently of the observation angles.

Each rotation stage is capable of 360 degrees of rotation, allowing the reflection and transmission to be observed at any angle. The rail rotation angle θ_D is considered to be at zero degrees when the transmission detector is at its leftmost position and would see the

beam passing through the leaf with no deflection. The leaf rotation angle θ_l is considered to be at zero degrees when the leaf surface is normal to the incident beam.

The motors of both the detector rail and leaf mount are controlled by an automated LabView® program which rotates the detectors and leaf to predetermined angles. At each set of angles the program takes 256 samples from each detector. The samples are then averaged, and a mean value is stored for each detector. The program then moves the leaf and/or detectors to the next set of angles, and the process is repeated until all the desired angle permutations are exhausted. Additionally, the entire procedure is repeated for four different leaves. The four mean values for each detector are then averaged into a single value for every angle permutation. The result is the average of 1024 samples taken from four different leaves. The additional data samples are collected in order to reduce any leaf-to-leaf variance in the final readings.

3.1.1 Speckle Reduction and Surface Averaging

The diameter of the Gaussian beam is optically set to approximately 1cm to provide a large illumination footprint. This is done for two reasons. First, laser speckle is reduced by increasing the size of the illumination beam. Reducing laser speckle in turn reduces variance in readings made by the detectors. Second, because a leaf's structure is not homogeneous (i.e., leaves have veins and stems, as well as other fine cellular structures running through them), it is important to illuminate a large enough area of the leaf to ensure good spatial averaging.

Speckle reduction and spatial averaging are also enhanced by periodically translating the leaf within the path of the beam. In addition to being mounted on a

rotation stage, the leaf is mounted on a vertical translation stage, shown in Figure 2, which is driven at a frequency of approximately 1 Hz. Translating the leaf up and down, coupled with the use of a broad illumination beam, creates a large effective area over which the leaf is sampled. As a result, localized leaf structure has minimal effect on the measurements.

3.1.2 Optical Fibers to delay the transit time of photons

The path of the beam tends a different optical path length from the laser to each of the different detectors. This difference in optical path length places the laser pulses at different temporal locations on the oscilloscope. In order to make the optical path lengths the same and line up the pulses, lengths of cable are added on to the detector to delay the transit time of the signal from each detector to the oscilloscope. Appendix Two includes a table of the measured optical path lengths of all the detector channels.

3.2 Leaf Data

BSDF data was collected from common maple and cottonwood leaves found in the Dayton, Ohio area during the weeks of May 21, 2006 and May 28, 2006. For each leaf species both the bidirectional reflectance (BRDF) and transmittance (BTDF) distribution functions were measured for incident angles of 0, 10, 20, 30, 40, 50, 60, 70, and 78 degrees. Illumination angles higher than 78 degrees were not used because the projected beam waist becomes larger than the physical width of the leaf as it rotates to higher angles. Scans for a single illumination angle then involves taking measurements of the scattered radiance at many detector angles about the leaf surface. We collected data at

detector angles spanning a range from -85 degrees to +85 degrees about the leaf surface normal, in increments of 5 degrees.

Because scattering properties change as leaves dry out, scan durations must be kept short.[9] Preliminary experiments showed a strong correlation between the freshness of a leaf and its scattering characteristics. For example, Figure 4(a) shows the BSDF of a fresh common maple leaf illuminated with normally incident light. The BSDF of the same maple leaf left out to dry overnight is shown in Figure 4(b). In these figures, light incident from the left (illustrated by the arrow) illuminates a leaf (bold line) at normal incidence. The resulting transmission profile (right hand lobes) and reflection profile (left hand lobes) are plotted in polar coordinates. There are appreciable effects due to leaf drying, as can be seen in the difference in the size of the reflection and transmission lobes between the two plots. In this case, as water in the leaf is replaced with air we observed that the reflectance of leaves increases while the transmittance decreases. Notice that the shape of the two lobes remains relatively constant, though the area encompassed by each changes appreciably.

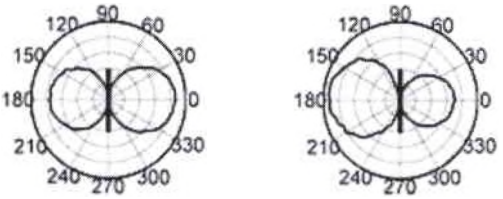

Figure 3.4 BSDF of (a) a fresh common maple leaf, and (b) an appreciably dried common maple leaf. Light, depicted by the arrow, is incident from the left and illuminates the leaf, portrayed by the solid line, at normal incidence.

Because of the effect of leaf drying on the scattering profile, it is necessary to ensure that the leaves remain fresh during the measurement procedure. In order to combat the

effects of leaf drying, a single leaf was used to scan only three illumination angles before it was replaced with a new, fresh leaf. As the scan of a single illumination angle takes approximately 25 minutes, limiting the use of a single leaf to less than 90 minutes proved short enough that drying effects were not noticeable in any leaves, or our final data.

3.2.1 Data Analysis

Polar plots of the BSDF data collected from maple leaves in the manner described above are provided in Figure 5. The laser beam (depicted by the arrows) was incident upon the leaves at θ_i angles of 0, 10, 20, 30, 40, 50, 60, 70, and 78 degrees. A separate sub-figure was made for each illumination angle. Each sub-plot has been normalized such that the sum of the areas of the transmission and reflection lobes is unity. Note that the scaling of the radial axis spans a range from 0 to 0.01 for each subplot, with exception of 78 degrees illumination which goes from 0 to 0.025.

The shape of the BRDF and the BTDF at normal incidence and low illumination angles appear to be largely Lambertian in nature. The radiated energy is located mostly along the leaf surface normal, decreasing cosinusoidally with the rotation of the detector angle. In addition, the shape of the BTDF remains relatively constant regardless of incident angle. However, as the incident angle increases past 50 degrees, the specular component of the reflection increases and the transmission decreases. The glint protrudes only slightly from the diffuse component at 50 degrees and becomes more pronounced as the incidence angle increases. At 78 degrees, the specular component dominates the diffuse reflection. Similar trends are seen in the cottonwood BSDF data shown in Figure 6. Because the maple and cottonwood data are so similar, from this point forward only

the maple leaf data will generally be discussed in detail. However, final results for both species of leaves will be presented throughout this article.

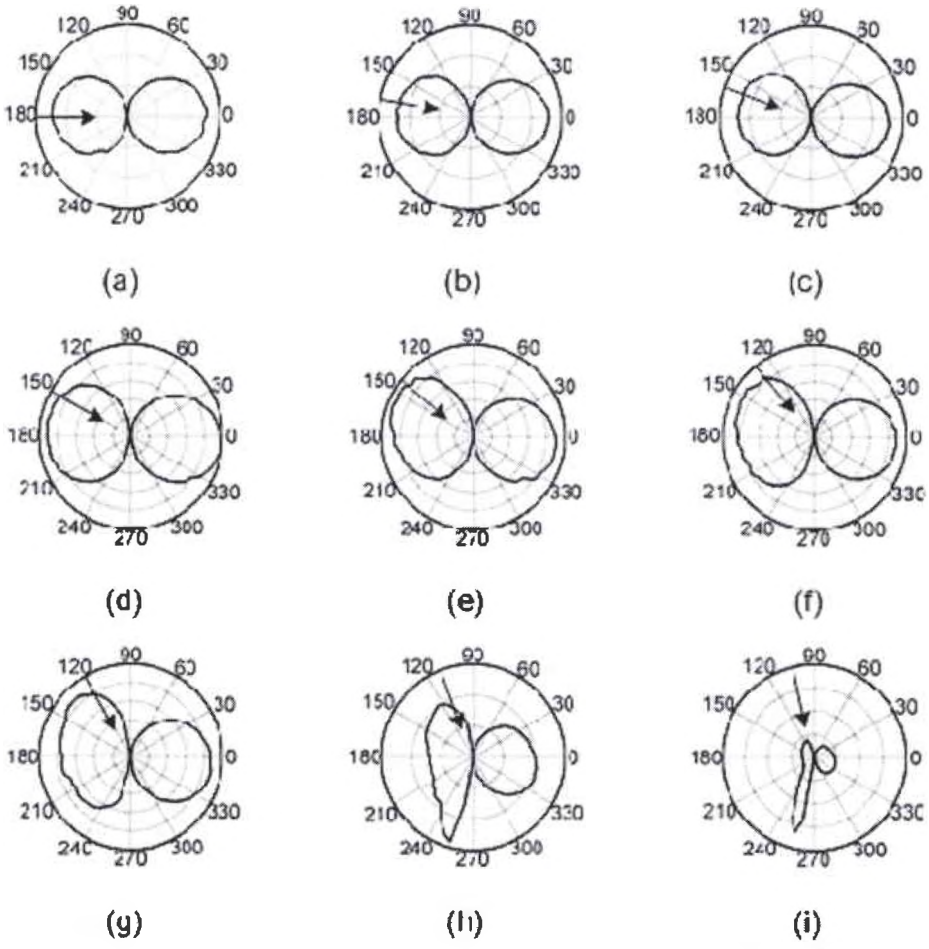

Figure 3.5 Measured BSDF data of common maple leaves for illumination angles θ_I of (a) 0 (b) 10 (c) 20 (d) 30 (e) 40 (f) 50 (g) 60 (h) 70 and (i) 78 degrees.

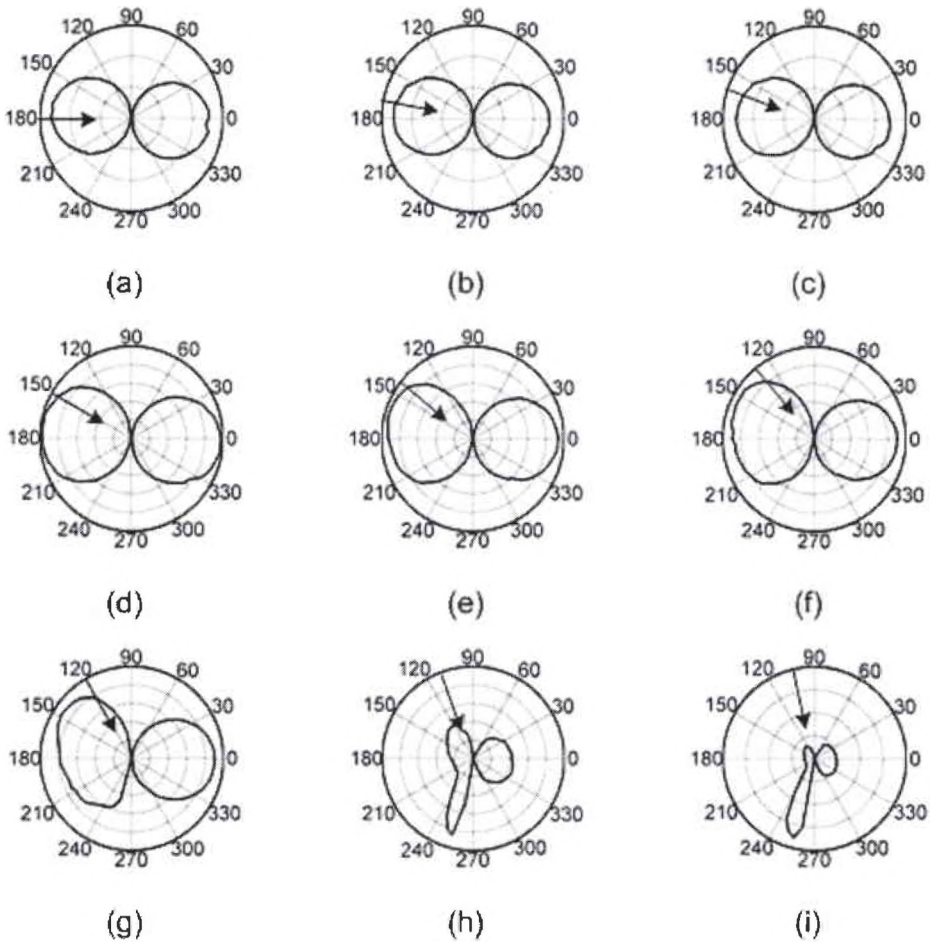

Figure 3.6 Measured BSDF data of cottonwood leaves for illumination angles θ_I of (a) 0 (b) 10 (c) 20 (d) 30 (e) 40 (f) 50 (g) 60 (h) 70 and (i) 78 degrees.

3.2.2 Calculation of Absorption Coefficient

Before investigating BRDF and BTDF features in more detail, it is important to determine the absorption coefficient $A_L(\theta_I)$ as a function of illumination angle. The method involves measuring the BRDF of a target with a known reflection coefficient R_S and comparing its area to that of the BRDF and BTDF of a leaf. A 60% reflective Spectralon® disc (i.e., $R_S = 0.60$ for all θ_I) was used as the standard of measure to which the scattering distributions of the leaves were compared. The normal illumination

BRDF of the Spectralon® disc is plotted, for example, along with the maple leaf BSDF for normal illumination in Figure 3.7. The area of each function is then calculated by integrating over the span of detector angles. That is, the area of the maple leaf BRDF is given by

$$A_R(\theta_I) = \int_{+90}^{+270} r_L(\theta_I, \theta_D) d\theta_D \,, \tag{3.1}$$

where $r_L(\theta_I, \theta_D)$ is the BRDF data measured at illumination angle θ_I and detector angle θ_D. Similarly, the area of the BTDF is given by

$$A_T(\theta_I) = \int_{-90}^{+90} t_L(\theta_I, \theta_D) d\theta_D \,, \tag{3.2}$$

where $t_L(\theta_I, \theta_D)$ is the BTDF.

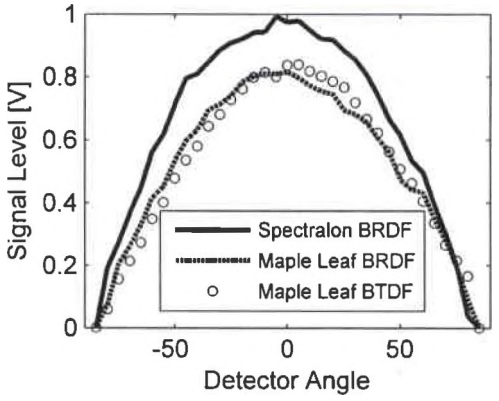

Figure 3.7 Comparison of the BSDF of maple and BRDF of spectralon.

The values of the reflection $R_L(\theta_I)$ and transmission $T_L(\theta_I)$ coefficients are directly related to the areas under the BRDF and BTDF curves. In particular, the ratio of the reflection coefficients for maple leaves and the Spectralon® disc is equal to the ratio of these areas according to the relationship:

$$\frac{R_L(\theta_I)}{0.60} = \frac{A_R(\theta_I)}{A_S}, \tag{3.3}$$

where A_S is the area of the spectralon BRDF at normal illumination. A similar expression can be written for the transmission coefficient:

$$\frac{T_L(\theta_I)}{0.60} = \frac{A_T(\theta_I)}{A_S}. \tag{3.4}$$

The absorption coefficient can then be found through the expression

$$A_L(\theta_I) = 1 - R_L(\theta_I) - T_L(\theta_I). \tag{3.5}$$

Tables 3.1 and 3.2 present values for the reflection, transmission, and absorption coefficients for maple and cottonwood leaves as a function of incident angle. Notice that the transmission coefficients decrease and the reflection coefficients increase with increasing illumination angle. This trend is also seen in the polar plots of the leaf BSDFs in Figures 3.5 and 3.6 where the size of the transmission lobe is seen to grow smaller with increasing illumination angle. Another trend evident in Tables 3.1 and 3.2 is the growth of absorption with illumination angle.

The relationship between illumination angle and the absorption coefficient for maple leaves is illustrated in Figure 3.8. A second order polynomial was fit to the data in order to allow the absorption coefficient for any illumination angle to be calculated. The following two equations, then, describe least square fit regression equations for the absorption coefficients of maple and cottonwood, respectively,

$$A_L(\theta_I) = -4.5156\times10^{-6}\times\theta_I^2 + 1.0373\times10^{-3}\times\theta_I + 25.415\times10^{-3} \text{ (maple)} \tag{3.6}$$

$$A_L(\theta_I) = 1.1885\times10^{-6}\times\theta_I^2 - 67.238\times10^{-6}\times\theta_I + 32.7\times10^{-3} \text{ (cottonwood).} \tag{3.7}$$

If desired, the reflection and transmission coefficients can be determined for any illumination angle by integrating the BRDF and BTDF models we will develop in the following sections.

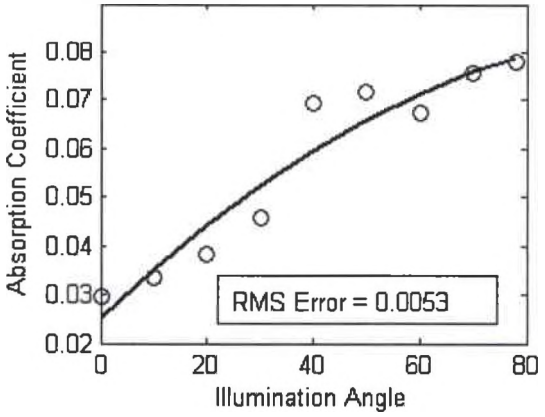

Figure 3.8 Absorptance as a function of illumination angle. The measured data (circles) is fit with a second order polynomial.

Table 3.1. Absorption as a function of illumination angle for maple leaves

I	R_L	T_L	A_L
0	0.4861	0.4841	0.0298
10	0.4879	0.4784	0.0337
20	0.4890	0.4727	0.0383
30	0.4884	0.4661	0.0456
40	0.4900	0.4406	0.0694
50	0.4984	0.4300	0.0716
60	0.5000	0.4327	0.0673
70	0.5009	0.4235	0.0756
78	0.5031	0.4188	0.0781

Table 3.2. Absorption as a function of illumination angle for cottonwood leaves

I	R_L	T_L	A_L
0	0.5414	0.4263	0.0323
10	0.5451	0.4227	0.0322
20	0.5500	0.4178	0.0322
30	0.5519	0.4160	0.0321
40	0.5548	0.4131	0.0321
50	0.5596	0.4084	0.0320
60	0.5457	0.4221	0.0322
70	0.5836	0.3847	0.0317
78	0.5801	0.3834	0.0365

3.2.3 Modeling Specular Reflection

In Figure 3.9(a), the maple leaf BRDF and BTDF for normally incident light are fitted with a cosine curve normalized to the integrated area of the measured data. The measured data is depicted by the circles, while the fitted curve is given by the solid line. The quality of the fit suggests that both the BRDF and BTDF are accurately modeled by a Lambertian distribution function for normal incidence. Similar results were seen for the other illumination angles less than 50 degrees. However, as the illumination angle increases beyond 50 degrees, other features become apparent. For example, plotted in Figure 3.9(b) are the 70 degree illumination angle BRDF and BTDF data fitted with normalized area cosine curves. While the transmission data remains nearly Lambertian, the reflection data exhibits other features that will be addressed in this section.

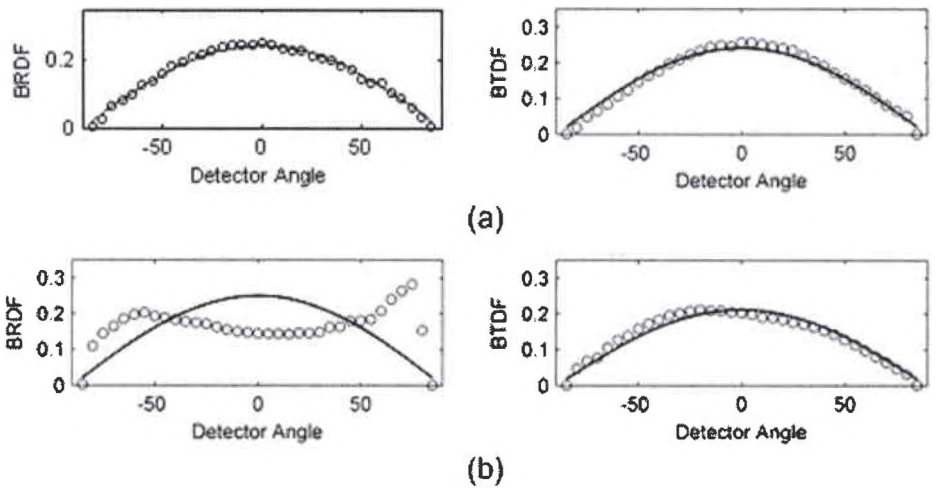

Figure 3.9 Lambertian fit to the BRDF (left) and BTDF (right) for (a) normal illumination and (b) illumination at 70 degrees.

Because of the irregularities in the shape of the reflection curves, it is difficult to model the BRDF data with a simple distribution. Also, the specular reflection peak at high incident angles makes it difficult to accurately replicate the curves by simply using high order polynomials. One approach to modeling the BRDF is to separate the specular and diffuse components. Accurate models individually representing the diffuse and specular profiles can then be found separately and later added together to produce the full BRDF model.

Under the assumption that the specular component is negligible for *detector angles* less than 40 degrees, the BRDF can be broken into two regions: one corresponding only to diffuse reflection ($\theta_D < 40$), and the other containing both specular and diffuse elements ($\theta_D > 40$). Separation of the two components in the latter region is then performed by fitting a polynomial curve to the known diffuse data and interpolating values within this region. Subtracting the interpolated diffuse data from the overlapping region leaves only the specular reflection component.

This process is illustrated in Figure 3.10 for maple leaf BRDF data taken at 70 degrees illumination angle. The non-separated BRDF data is depicted by the stars and circles, which in turn represent the diffuse and overlapping regions, respectively. A fourth order polynomial is fit to the diffuse data and represented by the solid line. The specular reflection component is then found by subtracting the diffuse reflection fit from the measured data. This is shown for the 50, 60, 70, and 78 degree illumination angles in Figure 3.11.

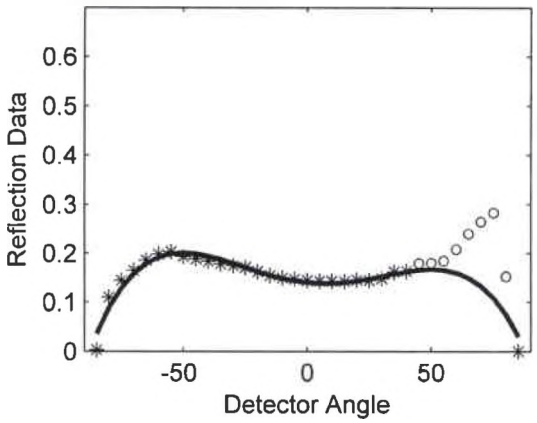

Figure 3.10 Separation of the diffuse and specular reflection components for 70 degrees illumination. The non-separated BRDF data is depicted by the stars and circles, which represent the diffuse and overlapping regions, respectively. A fourth order polynomial is fitted to the diffuse data and represented by the solid line.

As also shown in Figure 3.11, we found that the specular data is best fit with a normalized, reversed Rayleigh distribution of the form,

$$r_s(\theta_D) = F_S(\theta_I)\frac{(90-\theta_D)}{(90-\theta_P)^2}\exp\left[-\frac{(90-\theta_D)^2}{2(90-\theta_P)^2}\right], \tag{3.8}$$

where $F_S(\theta_I)$ is the fractional specular reflection, θ_D is the detector angle, and θ_P is the angle at which the function is a maximum. Interestingly, we found that a θ_P value of 75 degrees produced the best fit for all incidence angles.

The area of the reversed Rayleigh distribution must be normalized to the fractional area of the specular reflection peak before reconstructing the data with this model. Dividing the area of the specular reflection peak, $A_{RS}(\theta_I)$, by the total area of the reflection lobe, $A_R(\theta_I)$, for a given incident angle θ_I gives the fractional specular reflection according to

$$F_S(\theta_I) = \frac{A_{RS}(\theta_I)}{A_R(\theta_I)}. \tag{3.9}$$

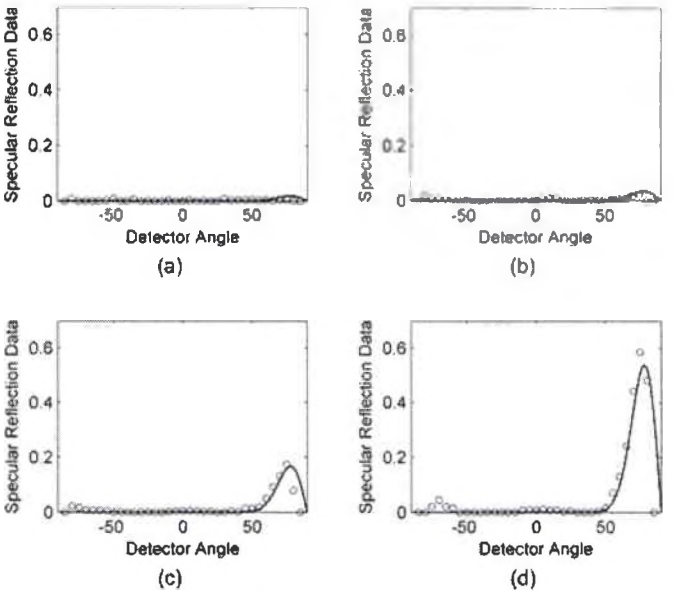

Figure 3.11 Normalized, reverse Rayleigh fits of the specular reflection data for illumination angles of (a) 50, (b) 60, (c) 70, and (d) 78 degrees.

As is seen in Figure 3.11, the fraction of specular reflection is dependent on the illumination angle. For illumination angles less than 50 degrees, specular reflection is negligible and $F_S\left(\theta_I \le 50^o\right)=0$. Moreover, at 90 degrees incidence it is assumed that all reflection is specular, yielding $F_S\left(90^o\right)=1$. Using these bounds, the fractional specular reflection was fit with a third order polynomial as shown in Figure 3.12 for maple leaves. The ratio of specular to total reflection for any illumination angle θ_I (in degrees) can then be written empirically as a piecewise continuous function according to the following equations provided for maple and cottonwood leaves, respectively,

$$F_S = \begin{cases} 0 & ,\theta_I < 50 \\ 12.7\times10^{-6}\times\theta_I^3 - 1.7\times10^{-3}\times\theta_I^2 + 77.2\times10^{-3}\times\theta_I - 1.19 & ,\theta_I \ge 50 \end{cases} \tag{3.10}$$

$$F_S = \begin{cases} 0 & ,\theta_I < 50 \\ -1.65\times10^{-6}\times\theta_I^3 + 922\times10^{-6}\times\theta_I^2 - 79.2\times10^{-3}\times\theta_I + 1.89 & ,\theta_I \ge 50 \end{cases} \tag{3.11}$$

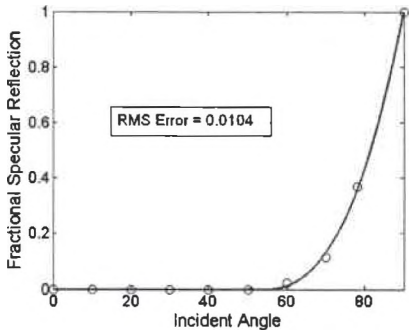

Figure 3.12 Fractional specular reflection as a function of incident angle. The measured data, depicted by the circles, is fit with a polynomial.

3.2.4 Modeling Transmission and Diffuse Reflection

Both the diffuse reflection and the transmission distribution functions are simply fit with polynomials such that when added to the Rayleigh model for specular reflection, the complete BSDF is reconstructed. Figure 3.13 shows the fitted data at an illumination angle of 70 degrees for common maple leaves. The transmission data is fit with a second order polynomial, while a fourth order polynomial is used for the diffuse reflection. A higher order polynomial is needed for diffuse reflection because the structure of the distribution becomes somewhat more complex at higher incident angles. When the specular reflection component is then added to the corresponding polynomials modeling diffuse reflection, the complete BRDF is reconstructed, as shown for maple leaves in Figure 3.14.

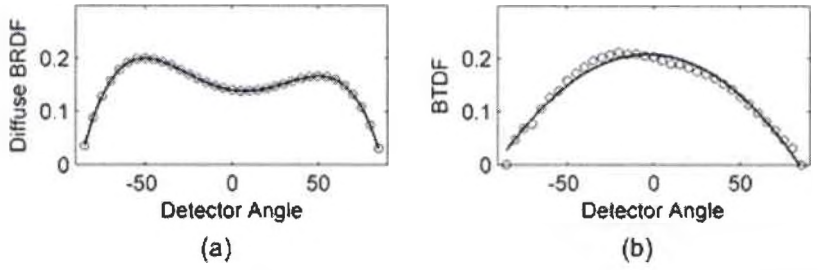

Figure 3.13 Fitted maple leaf BSDF curves for illumination at 70 degrees. (a) The diffuse reflection data is fit with a 4th order polynomial while (b) the transmission data is fit with a 2nd order polynomial.

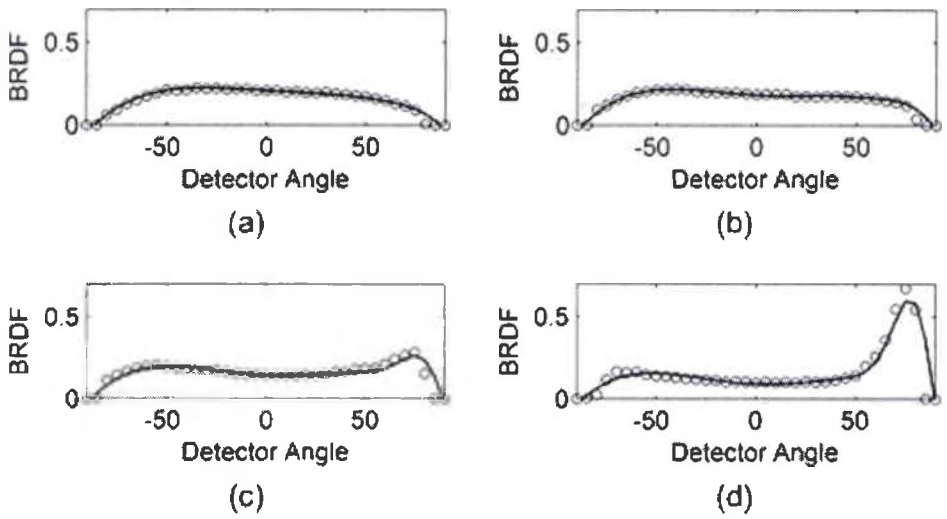

Figure 3.14 BRDF reconstructed by summing the diffuse and specular components for (a) 50, (b) 60, (c) 70, and (d) 78 degrees illumination.

3.2.5 Leaf Data Interpolation

The ability to accurately estimate the BSDF for any illumination angle will be a valuable resource. Thus far, it has been shown that scattering data at the measured illumination angles can be reconstructed using simple polynomial fits and, for high illumination angle BRDF's, a reversed Rayleigh distribution. However, filling in the gaps for intermediate illumination angles requires creating an additional fit to the modeled data. As discussed in the previous two sections, for a given incidence angle, the polynomial equations used to describe the BTDF and diffuse BRDF as a function of both detector θ_D and illumination θ_I angles are given, respectively, by:

$$t(\theta_D, \theta_I) = p_{1t}\theta_D^2 + p_{2t}\theta_D + p_{3t} \tag{3.12}$$

$$r_d(\theta_D, \theta_I) = p_{1r}\theta_D^4 + p_{2r}\theta_D^3 + p_{3r}\theta_D^2 + p_{4r}\theta_D + p_{5r}, \tag{3.13}$$

where the polynomial coefficients, p, are dependent on the illumination angle. With knowledge of these coefficients, the BTDF and diffuse BRDF data can be interpolated at

intermediate detector angles for a previously examined illumination angle. However, in order to interpolate BTDF and diffuse BRDF data at intermediate illumination angles it is necessary to examine the relationship between θ_l and the value of each of the p-coefficients. Fitting p as a function of θ_l will allow the interpolation of p at intermediate illumination angles.

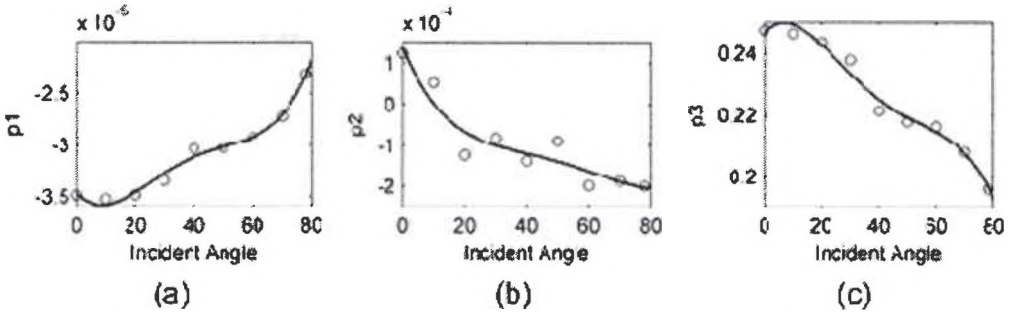

Figure 3.15 Fit of the 0th, 1st, and 2nd order p-coefficients describing the transmission data for maple leaves.

In Figure 3.15, the p-coefficients of the maple leaf BTDF data are shown fit with a fourth order polynomial. In general, the fourth order polynomial fits to the p-coefficients for both BTDF and diffuse BRDF data is defined by a set of five q-coefficients according to

$$p_{ix}(\theta_l) = q_1\theta_l^4 + q_2\theta_l^3 + q_3\theta_l^2 + q_4\theta_l + q_5, \tag{3.14}$$

where, for transmission, $i = 1,2,3$ and $x = t$, and for reflection, $i = 1,2,3,4,5$ and $x = r$. Knowledge of the q-coefficient values then allows one to calculate the p-coefficients for any illumination angle through Equations 3.12 and 3.13. The q-coefficients calculated for the transmission and diffuse reflection maple leaf data are shown in Tables 3.3 and 3.4, respectively. Similarly, values for the cottonwood q-coefficients are provided in Tables 3.5 and 3.6.

Using this method of data interpolation we have examined the BSDF estimates at each of the angle permutations used during the data acquisition procedure. The RMS errors found between the originally measured data and the estimates generated through this interpolation method were found to be approximately 2.5% and 1.0% for the BRDF and BTDF of maple leaves, respectively. The corresponding RMS errors calculated for cottonwood leaves were approximately 3.7% and 1.2%.

Table 3.3. Table of q-coefficients defining the p-coefficient of transmission for maple leaves.

	q_{1t}	q_{2t}	q_{3t}	q_{4t}	q_{5t}
p_{1t}	3.0388e-012	-463.75e-012	23.428e-009	-300.83e-009	-3.4701e-006
p_{2t}	34.837e-012	-7.1221e-009	517.86e-009	-17.93e-006	135.77e-006
p_{3t}	-10.371e-009	1.6844e-006	-89.529e-006	1.0167e-003	246.48e-003

Table 3.4. Table of q-coefficients defining the p-coefficient of diffuse reflection for maple leaves.

	q_{1r}	q_{2tr}	q_{3r}	q_{4r}	q_{5r}
p_{1r}	1.2954e-015	-180.66e-015	6.8481e-012	-132.35e-012	120.16e-012
p_{2r}	25.825e-015	-5.0125e-012	285.57e-012	-3.6431e-009	32.217e-009
p_{3r}	-10.817e-012	1.5674e-009	-58.687e-009	1.0776e-006	-34.531e-006
P_{4r}	-123.8e-012	23.992e-009	-1.2636e-006	8.0717e-006	-164.4e-006
P_{5r}	-6.2703e-009	369.59e-009	-12.501e-006	-257.65e-006	245.19e-003

Table 3.5. Table of q-coefficients defining the p-coefficient of transmission for cottonwood leaves.

	q_{1t}	q_{2t}	q_{3t}	q_{4t}	q_{5t}
p_{1t}	2.5913e-012	-391.07e-012	17.815e-009	-191.88e-009	-34.326e-006
p_{2t}	4.4203e-012	-4.1417e-009	325.17e-009	-4.7745e-006	-168.86e-006
p_{3t}	-9.2296e-009	1.499e-006	-75.217e-006	738.91e-006	245.53e-003

Table 3.6. Table of q-coefficients defining the p-coefficient of diffuse reflection for cottonwood leaves.

	q_{1r}	q_{2tr}	q_{3r}	q_{4r}	q_{5r}
p_{1r}	2.1389e-015	-272.67e-015	8.6857e-012	-111.72e-012	1.6618e-009
p_{2r}	-59.223e-015	7.1463e-012	-208.54e-012	1.3098e-009	37.969e-009
p_{3r}	-18.62e-012	2.5167e-009	-85.345e-009	1.098e-006	-47.705e-006
P_{4r}	479.27e-012	-62.848e-009	2.2671e-006	-23.813e-006	-355.59e-006
P_{5r}	5.4467e-009	-1.4462e-006	62.194e-006	-993.25e-006	261.58e-003

3.2.6 Procedure for Constructing the BSDF

BSDF values at any set of angles (θ_I, θ_D) can be accurately estimated for both maple and cottonwood leaves from the information provided herein. Using the following procedure, surface fits for both the BRDF and BTDF can be interpolated for illumination angles spanning a range from 0 to 78 degrees. These are plotted for maple leaves, for example, in Figures 3.16 and 3.17, respectively. The RMS errors of the surface fits of the BRDF and BTDF are 0.0254 and 0.0103, respectively.

1) Using Equations 3.6 or 3.7, calculate the absorption coefficient, $A_L(\theta_I)$

2) Using Equations 3.12 and 3.14, calculate the BTDF, $t(\theta_D, \theta_I)$. The coefficients required for these equations are found in Tables 3.3 and 3.5 for maple and cottonwood leaves, respectively.

3) Using Equations 3.13 and 3.14, calculate the diffuse BRDF, $r_d(\theta_D, \theta_I)$. The coefficients required for these equations are found in Tables 3.4 and 3.6 for maple and cottonwood leaves, respectively.

4) Generate the specular BRDF, $r_s(\theta_D, \theta_I)$, using Equation 3.8. Normalize the function to the fractional specular reflection calculated from either Equation 3.10 or 3.11 for maple and cottonwood leaves, respectively.

5) Construct the complete BRDF by adding together the specular and diffuse components. That is,

$$r_L(\theta_D, \theta_I) = r_d(\theta_D, \theta_I) + r_s(\theta_D, \theta_I). \tag{3.15}$$

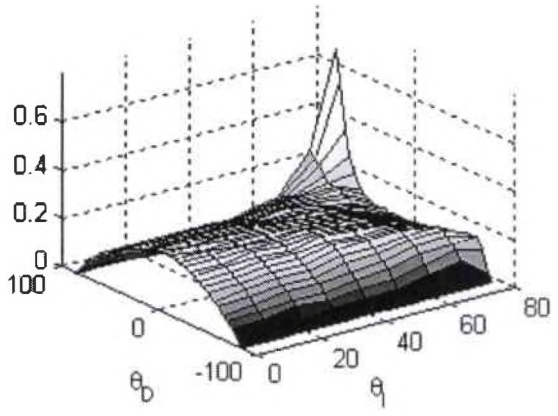

Figure 3.16 Surface fit of the BRDF.

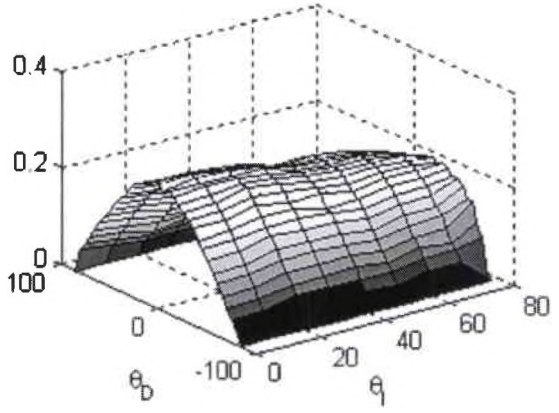

Figure 3.17 Surface fit of the BTDF.

Note that the BRDF and BTDF have been normalized in such a way that the sum of their areas plus the absorption coefficient calculated in step (1) is equal to unity. That is,

$$1 = \int_{-90}^{90} t(\theta_D, \theta_I) d\theta_D + \int_{90}^{270} r_L(\theta_D, \theta_I) d\theta_D + A_L(\theta_I). \tag{3.16}$$

The above steps present a stand-alone method for generating the BSDF of maple and cottonwood leaves for any illumination angle. This method is appropriate for use in

The above steps present a stand-alone method for generating the BSDF of maple and cottonwood leaves for any illumination angle. This method is appropriate for use in remote sensing models where probability density functions describing the scattering by individual leaves must be considered (e.g., in Monte Carlo simulations). Such models typically require examination of the scattering pdfs in both the zenith and azimuth angles. While our models have been developed based only upon in-plane measurements, they may be extended to allow out of plane estimates by assuming azimuthal symmetry in both the diffuse BRDF and the BTDF. We address the asymmetry of the specular component by forcing the azimuth angle to be equal to the angle of incidence in the case of specular reflection.

Chapter 4

Canopy Modeling

Modeling the propagation of light through a tree canopy is a very complex technique, in which an incident beam of photons is progressively scattered through a random medium consisting of leaves. Canopies are generally modeled as a collection of scatterers which are randomly oriented spatially and angularly throughout the canopy. Analytically solving for such a system is essentially impossible. The problem of multiple scattering through a random medium is best approached through Monte Carlo methods on a photon by photon basis. The advantage of using Monte Carlo methods is that multiple scatterings can be calculated without complex analysis, as only the single scattering probability functions are required. Also, this method is robust in terms of handling various forms of canopy parameters describing the random medium.

In Monte Carlo methods, the multiple scattering events in the canopy are treated as a sequence of interactions between a single photon and a discrete scatterer. The simplification lies in the fact that the end result of photon scattering through a canopy does not come from looking at the canopy as a whole, but looking at each photon on an individual basis and each interaction one at a time.

The canopy model considered in this project assumes a cylindrical canopy of radius 30 meters and height of 15 meters, in accordance with several accepted values.[22, 31, 41] A pencil beam is incident at the center of the roof of the canopy such that initial photons have a zenith angle orientation of 0 degrees. Here, the zenith angle, θ_i, is defined to be 0 degrees looking straight down and 90 degrees looking horizontally through the canopy. Upon propagating through the canopy, a light beam will experience spatial, angular, and temporal spreading. As each photon propagates through the canopy it gets bounced around spatially and angularly by the leaves. The beam of photons exiting the canopy will be physically wider, decollimated, and temporally dispersed from the incident beam as illustrated in Figure 4.1.

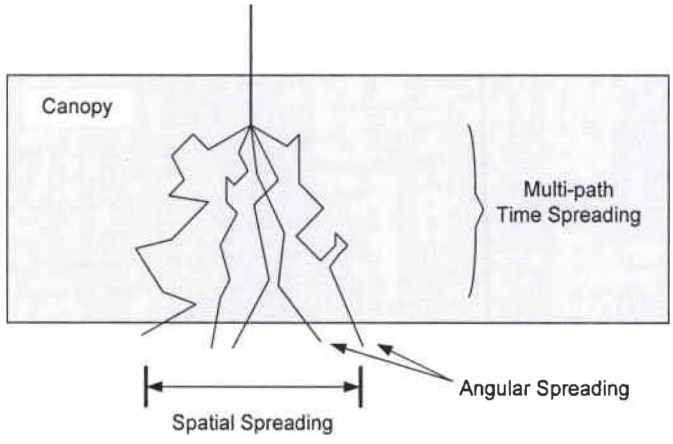

Figure 4.1 An incident light beam is dispersed spatially, angularly, and temporally

4.1 Random Walk

The algorithm we used for tracing the paths of photons through the canopy is based on the cloud propagation model presented by E. Bucher[8], and depicted in the flow

chart found in Figure 4.2. A single incident photon enters the canopy and travels a distance d_1 before it is scattered by the first leaf. The boundary conditions must then be checked to see if the photon has left the canopy. If it has, spatial, angular and temporal data is saved for the photon and a new photon is launched into the canopy. If the photon has not left the canopy, random leaf orientation angles are selected. The illumination angle is then calculated by finding the angle made between the leaf normal vector and the current propagation direction of the photon. Using the corresponding BSDF, scattering angles are randomly selected from the leaf. The new propagation direction is then calculated from the geometrical relationship between the leaf orientation angles and the scattering angles. The photon then travels a distance d_2 in the new direction to the next randomly oriented leaf, and the process is repeated.

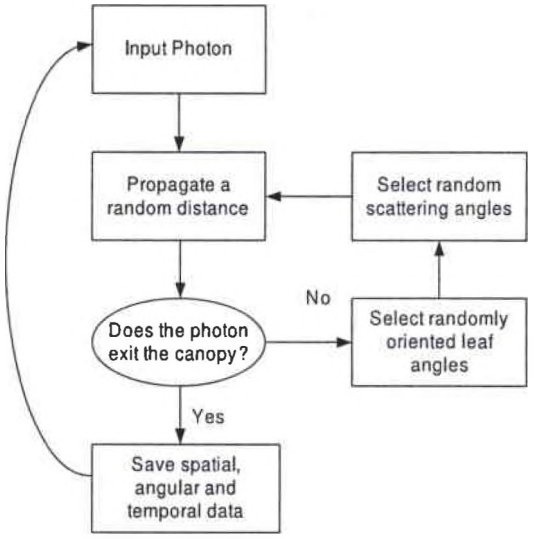

Figure 4.2 Random walk flow chart

The algorithm discussed above is referred to as a random walk, as each individual photon is randomly stepped through the canopy. The photon can go any distance in any direction determined by a number of random variables which must be examined at each

step. Each of the random variables is governed by a probability density function which will randomly distribute the variable in some form. Therefore, the canopy is described completely by the probability density functions describing the following canopy variables:

i. The angular orientation of the scatterers (θ_l and ϕ_l)

ii. The random distance to the next scattering event (d)

iii. The probability that the photon is scattered or absorbed (R, T, A)

iv. The angular orientations of the photon exiting from the scattering event (θ_s and ϕ_s)

4.2 Leaf Angle Orientations

The main function of leaves is to gather sunlight for photosynthesis. Therefore, the leaves of a canopy are angled such that most of their surface is facing towards the sun. In the instance of a single tree, the leaves near the top of the tree are nominally facing straight upwards, while the leaves on the outer edges typically point radially away from the tree trunk. However, when a tree is placed within a canopy, there is no "edge" of the canopy, and therefore the nominal leaf angle is always facing straight up. Of course, there is some statistical variation among the leaves which can be described by the pdfs below.

It is most typical to assume that the leaf azimuth orientation distribution is independent of the leaf zenith angle distribution, and therefore may be selected independently. Most often the azimuth distribution is assumed to be uniform on the range $[0, 2\pi]$[8, 22], that is

$$p_{\Phi_L}(\phi_l) = \frac{1}{2\pi}[u(\phi_l) - u(\phi_l - 2\pi)]. \tag{4.1}$$

Generation of random leaf azimuth angles is a simple transformation, as both the random number generator in Matlab and the leaf azimuth pdf are uniformly distributed. If x is a uniformly random number on the interval $[0,1]$, then the transformation to the uniformly random leaf azimuth on the interval $[0,2\pi]$ is given by,

$$\phi_l = 2\pi x. \tag{4.2}$$

The zenith angle pdf is chosen to be cosinusoidal in accordance with McDonald, Dobson, and Ulaby[15]. The leaves are mostly horizontal and almost never vertical. The leaf angle is described by its area normal vector, $\hat{a}_N$, which in this case has a cosine distribution:

$$p_{\Theta_L}(\theta_l) = \cos\theta_l \left[u(\theta_l) - u\left(\theta_l - \frac{\pi}{2} \right) \right]. \tag{4.3}$$

The transformation of a uniformly random number on the interval $[0,1]$ to a cosinusoidal distribution on the interval $\left[0, \frac{\pi}{2}\right]$ was performed in Section 2.1.5 and is given to be

$$\theta_l = \text{asin}(x). \tag{4.4}$$

Because the leaf orientation angles are generated in the reference frame of the canopy, and not in the direction of the photon propagation (see Figure 4.3), it is necessary to calculate the angle of incidence between the leaf and the incoming photon. The derivation of this angle is found in Appendix E.

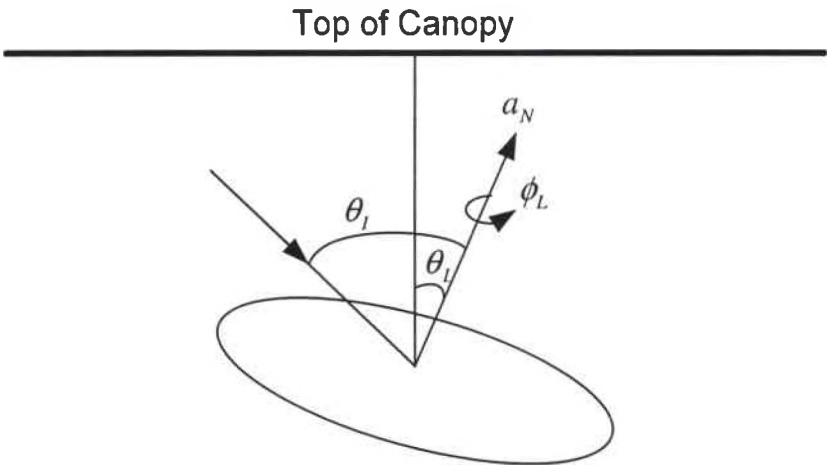

Figure 4.3 Angular orientation of leaves in the canopy.

4.3 Random Propagation Distance

For a *homogeneous* medium of constant number density, the distance d_j that the photon travels between the $(j-1)$th and jth scattering events is randomly selected with a negative exponential probability density function[16]:

$$p_d(d) = \frac{1}{D}\exp\left[-\frac{d}{D}\right]. \tag{4.5}$$

The random variable d assumes values between d and $d+\Delta d$ with a total probability $\frac{1}{D}\exp\left[-\frac{d}{D}\right]\Delta d$. That is, the random distance to the next scatterer, d, is on average D. The scaling parameter D for the negative exponential is the mean free path of the photon, which in turn is dependent upon the mean projected area $\bar{A}_p(\theta_l)$ and leaf number density $N_v(z)$.

4.3.1 Mean Projected Area, $\overline{A}_p(\theta)$

When an object is viewed from an angle different from that of the surface normal, it is not the actual area of the object that is important, but the projection of the object's actual area in the direction of viewing. The projected area $A_p(\theta_l)$ of the object at the look angle θ is what the viewer sees the area of the object to be. Illustrated in Figure 4.4, the projected area seen by the viewer is related to the actual area of the object A by the cosine of the angle made between the viewer and the surface normal.

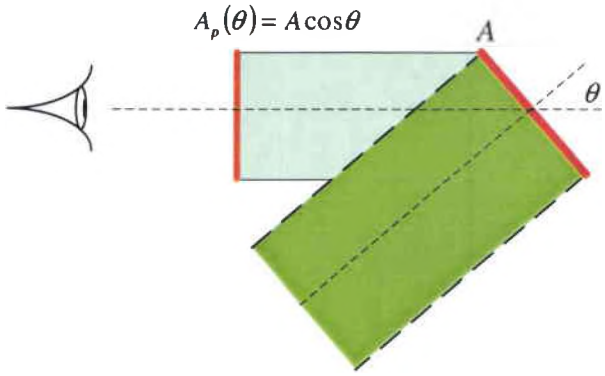

Figure 4.4 The projected area is the area of the object as a see from some viewing angle θ

For the case where the angular orientation of the object is constant such a calculation is very simple to make. However, in the case of the canopy propagation model, the angular orientation of the leaf is randomly distributed. The leaf may take on a number of possible orientations, thus the viewing angle θ_l is unknown. A new quantity must be created to account for all possible leaf orientations. The mean projected area $\overline{A}_p(\theta_l)$ is the average value of projected area a viewer observing the canopy at an angle of θ_l would expect to see. Mean projected area is derived in Appendix Three by integrating the projected area over all possible angular orientations of the leaf. Assuming

that the leaves are modeled as circular discs of diameter d $\left(\text{Area} = A_L = \frac{\pi d^2}{4}\right)$, the expression for the mean free path is found to be:

$$\bar{A}_p(\theta_l) = \frac{d^2}{4}\left[\sin\theta_l + \frac{\pi^2}{4}\cos\theta_l\right]. \tag{4.7}$$

Not surprisingly, the final result for the mean projected area is a function of look angle. Depending on which direction a photon is propagating in the canopy, it will see a different mean projected area. A photon traveling horizontally through the canopy will see a much smaller projected area than will a photon traveling vertically. This disparity arises because the most preferred orientation of a leaf is horizontal, which projects most of its area upward. A photon traveling horizontally sees mostly leaf edges and very small areas. Similarly, a photon traveling vertically will see mostly leaf areas and very rarely leaf edges.

4.3.2 Leaf Number Density, $N_V(z)$

For many random media, such as clouds or gases, the distribution of scatterers is homogeneous throughout the medium. In such cases, the number density of scattering events is a constant. However, it is not so simple in the case of a canopy, as the number density of leaves varies as a function of height. There are many papers that attempt to characterize the distribution of leaves within a canopy. It is common convention that a canopy has azimuthal symmetry and leaf distribution is independent of horizontal displacement.[22] It is also accepted that the distribution of leaves varies as a function of vertical height within the canopy as shown in Figure 4.5.[1,17,27] A great number of papers have been published in which the vertical profiles of canopies have been examined. Ross

and Ross, and Lalic and Mihailovic characterize the vertical profile of a canopy in terms of leaf area density $L(z)$, which is a measure of total leaf area [m^2] contained within a volume [m^3] of canopy.[1, 28] This is a convenient way to characterize the leaf distribution in a canopy is to use the leaf area density, as leaf area density is converted to leaf number density by multiplication of the LAD function by the average area of each leaf.

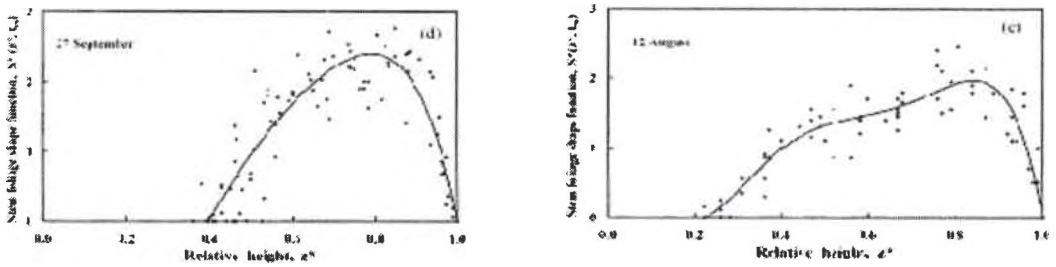

(a) (b)

Figure 4.5 Leaf distribution as a function of relative canopy height for Willow Coppice during (a) September, and (b) August of 1998 [27]

The vertical distribution of the leaf-area density (LAD) is difficult to be either measured precisely or estimated.[30] An analytic derivation of a function describing the vertical leaf profile of a canopy is impossible to create. A more appealing method is to derive an empirical expression for $L(z)$. Lalic and Mihailovic introduce a simple empirical formula for $L(z)$ based on three forest parameters already archived.[1] Derivation of an expression modeling measured LAD data is based on canopy height h, maximum value of leaf-area density L_m, and corresponding canopy height z_m. It is found that the leaf-area density distribution $L(z)$ can be properly described by the function having the following form:

$$L(z) = L_m \left(\frac{h - z_m}{h - z} \right)^n \exp\left[n \left(1 - \frac{h - z_m}{h - z} \right) \right], \tag{4.8}$$

where

$$n = \begin{cases} 6 & 0 \le z < z_m, \\ \frac{1}{2} & z_m \le z \le h. \end{cases}$$

As was mentioned before, the values of h, L_m, and z_m can be obtained from a forest parameter database. Some values for these parameters are given in Table 4.1.

Table 4.1: Some values for the parameters defining the LAD function

	L_m	z_m/h
Common Maple 1	1.45	0.85
Common Maple 2	1.06	0.70
Common Maple 3	2.18	0.70
Silver Birch 1	1.6	0.80
Oak 1	1.9	0.80
Pine 1	1.4	0.75
Pine 2	0.16	0.60
Pine 3	0.37	0.60

Dividing the leaf area density by the leaf area A_L will give the leaf number density as a function of relative canopy height:

$$N_V(z) = \frac{L(z)}{A_L} = \frac{4}{\pi d^2} L_m \left(\frac{h - z_m}{h - z}\right)^n \exp\left[n\left(1 - \frac{h - z_m}{h - z}\right)\right], \tag{4.9}$$

where,

$$n = \begin{cases} 6 & 0 \le z < z_m, \\ \frac{1}{2} & z_m \le z \le h. \end{cases}$$

4.3.3 Mean Free Path

The mean free path of a photon is the average distance traveled by the photon before it encounters another scattering event. It varies as a function of both the number density of leaves in the region surrounding the photon and by the projected area of the

leaves in the direction of the photon. The mean free path can be expressed as the inverse product of the mean projected area and the leaf number density:

$$D(z,\theta)=\frac{1}{\bar{A}_p(\theta)\cdot N_V(z)} \tag{4.6}$$

Inserting the expressions for mean projected area and leaf number density into Equation 4.6 gives the mean free path of a photon as a function of canopy height and look angle. After simplification the average distance traveled by a photon in the direction θ through a homogeneous medium with number density found at the height z is given by,

$$D(z,\theta)=\frac{\pi}{\left[\sin\theta+\frac{\pi^2}{4}\cos\theta\right]\cdot L_m\left(\frac{h-z_m}{h-z}\right)^n \exp\left[n\left(1-\frac{h-z_m}{h-z}\right)\right]}. \tag{4.11}$$

4.3.4 Reverse Transformation of Random Propagation Distance

Recall the discussion on computer random number generators and the transformation of a uniform random variable to another random variable in Section 2.1.4. To select a random propagation distance into the canopy from the height z in the direction of the zenith angle θ, the uniform random variable created in Matlab must be converted to follow the probability density function expressed in Equation 4.5.

Let x be a uniform random number distributed on the interval $[0,1]$. The first step to changing the variable is that the pdf must be converted into the corresponding cumulative distribution function by integration.

$$F_d(d)=\frac{1}{D}\int_0^d \exp\left[-\frac{d}{D}\right]dd=\frac{1}{D}\left(-D\exp\left[-\frac{d}{D}\right]\right)_0^d$$

$$F_d(d) = 1 - \exp\left[-\frac{d}{D}\right] \tag{4.12}$$

The relationship between x and d is such that $x = F_d(d)$, which means that,

$$d = F_d^{-1}(x)$$

Solving for the inverse of the cdf gives

$$d = -D\ln(1-x). \tag{4.13}$$

Equation 4.13 gives the expression for calculating a random value for the propagation distance of a photon through a homogeneously distributed canopy. Note the expression derived above assumes that the canopy is homogeneously distributed, or equivalently that the mean free path is constant throughout the canopy, which is not the case. Section 4.3.7 examines the steps that must be taken to propagate a photon through an inhomogeneously distributed region.

4.3.5 Non-uniform LAD

The random propagation distance given in Equation 4.13 is only valid for homogeneous media where there is a *constant number density* of scatterers throughout the entire medium. The problem lies with using an instantaneously calculated leaf number density to represent the number density of the entire canopy. Because the LAD varies as a function of canopy height, the mean free path needs to be recalculated periodically as the photon travels through the canopy. A method for propagating a photon through an inhomogeneously distributed medium, i.e. canopy, is devised such that the mean free path is recalculated periodically as the photon travels through the canopy. This method involves breaking the canopy into regions where the number density remains

relatively constant throughout the region. The inhomogeneous canopy is then treated as a collection of many smaller homogeneous canopies stacked one on top of the other.

The canopy is divided into 50 regions with variable spacing such that the change in LAD from the beginning to the end of the same region is negligible. Areas where the LAD changes rapidly will have smaller regions and areas where LAD does not change much at all will have broadly spaced regions. The calculation of the region spacing is based on the derivative of the LAD function, which is derived in Appendix Four and found to be

$$\frac{d}{dz}L(z) = L_m\left(\frac{z_m}{z}\right)^n n\left[z^{-1} + z_m z^{-2}\right]\exp\left(n\left(1-\frac{z_m}{z}\right)\right). \tag{4.14}$$

Calculating the spacing of the regions of the canopy is performed by integrating the area under the dLAD curve and dividing the total area by the number of regions. The canopy is then broken into regions such that each region has area equal to this quantity, which ensures that the total change in LAD across each region is equal. Thus, regions where the LAD does not change rapidly are large and regions where the LAD does change rapidly are small.

Figure 4.6 shows a comparison of 50 discretized regions (blue) to the smooth leaf area density curve (red). Notice that as the LAD curve levels out near the bottom of the canopy ($T - z \approx 7$), the length of region spacing increases greatly. Only a few regions are needed to characterize this part of the curve as the leaf area density remains relatively constant over this span of the canopy. In contrast, examine the top of the canopy, where the LAD function is changing very rapidly. The spacing of the regions in this part of the canopy is very small. Because the LAD of the canopy is changing so rapidly here, very small regions must be created to keep the LAD constant within each region.

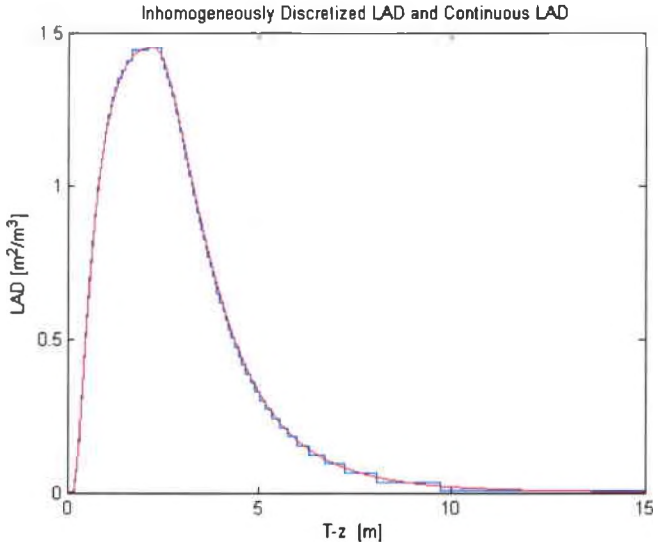

Figure 4.6 Comparison of the discrete LAD function created with non-uniformly spaced regions (blue) and the continuous LAD function defined by Lalic and Mihailovic[1].

4.3.6 Region to region propagation

There is now assumed to be a homogeneous distribution of leaves within each region. Therefore the propagation of a photon within a single region can be performed using the probability density function given in Equation 4.5. If the randomly selected propagation distance calls for a leaf interaction before the photon exits the current region, then that is the location of the next scattering event. However, if the projected propagation distance is greater than the current region spacing, the photon propagates to the edge of the next region. The mean free path must be recalculated for the new region and a new propagation distance is calculated. Once again, the photon can interact with a leaf within the current region, or propagate to the edge of the next region. The process is repeated until the photon has an interaction.

For example, assume that a photon is in the f th region heading in the $+z$ direction towards the $(f+1)$th region, as seen in Figure 4.7. Also assume the photon is

initially located inside the region (not at the beginning or end but somewhere in the middle) and is propagating in the direction of the angle θ. The distance between the current location of the photon and the end of the f th region is calculated in the z direction and given by df. Generate the projected propagation distance dp using the mean free path of the f th region and Equation 4.5. The projected propagation distance is then the distance that the photon would travel before interaction in an infinite homogeneous medium of constant LAD found in region f. Because the extent of the region is finite, and propagation beyond the current region requires the recalculation of the leaf area density, the projected propagation distance is only a projection of the possible propagation distance of the photon.

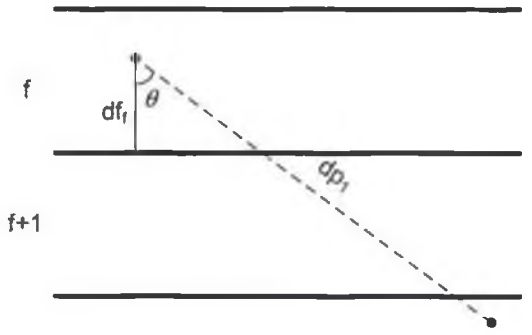

Figure 4.7 Projected propagation distance, dp, of a photon in a region with constant leaf area density, f.

There are two possibilities after calculating dp_1: (1) $dp_1 \cdot \cos\theta < df_f$, in which case the photon has not left the f th region, or (2) $dp_1 \cdot \cos\theta \geq df_f$, in which case the photon has left the f th region. For the first case, the photon interacts with a leaf before it leaves the region. In this case, the projected propagation distance dp_1 becomes the actual

propagation distance d. The new spatial location of the photon at this interaction can be calculated. From there, the photon is scattered as normal from the leaf.

For the second case, the photon does not interact with a leaf before it leaves the region. Because the projected propagation is only valid for the f th region, the actual propagation distance is set to

$$dp_1 = \left| \frac{df_f}{\cos\theta} \right|, \tag{4.15}$$

which puts the photon at the edge of the f th and $(f+1)$th regions. The absolute value is used in this equation to account for both upward and downward traveling photons. Using the leaf area density of the $(f+1)$th region randomly select a new projected propagation distance dp_2, as is done in Figure 4.8.

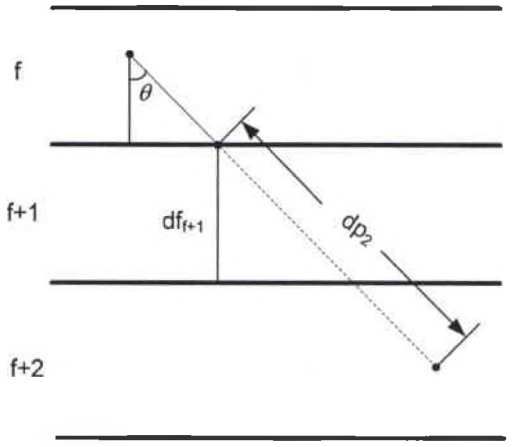

Figure 4.8 Continued propagation of a photon through the changing regions of different leaf area density. A new projected propagation distance,

Once again, there are two possibilities: (1) $dp_2 \cdot \cos\theta < df_{f+1}$, where the photon has not left the $(f+1)$th region, or (2) $dp_2 \cdot \cos\theta \geq df_{f+1}$, where the photon has left the $(f+1)$th region. For the first case, the photon interacts with a leaf before it leaves the

region. The projected propagation distance is then added to the current actual propagation distance to give an updated actual propagation distance of $d = dp_1 + dp_2$. For the second case, as shown in Figure 4.6, the photon exits the region. Once again, because the projected propagation is valid only for the current region, a new dp_j value must be calculated for the next region. Store the second projected propagation distance for later analysis:

$$dp_2 = \left| \frac{df_{f+1}}{\cos\theta} \right|. \tag{4.16}$$

The above steps must be repeated until the projected propagation distance gives an interaction within the current region of the photon. The final actual propagation distance is then calculated by summing all the dp terms together,

$$d = \sum_{j=1}^{J} dp_j \tag{4.17}$$

4.4 Reflection, Transmission and Absorption

The probability of a single photon being reflected, transmitted or absorbed by a leaf is determined by the reflection and transmission coefficients, which are calculated in Section 3.2.2. The random selection of reflection, transmission or absorption from a leaf is done by creating a random number uniformly distributed between 0 and 1. Assign absorption to the values between 0 and A, transmission to the values between A and A+T, specular reflection to the values between A+T and A+T+R*F_s and diffuse reflection to the values between A+T+R*F_s and 1. The vale F_s is the fractional specular reflection, which is calculated from Equations 3.10 and 3.11 for maple and cottonwood,

respectively. Whatever region the random number falls within determines the scattering property of the photon at that leaf. Selection of scattering in this way will uniformly randomly select whether the photon is absorbed, transmitted or reflected at each leaf.

4.5 Scattering Angle

The scattering angles from the leaf are defined as shown in Figure 4.9. Note that the scattering zenith angle is the same as the detector angle from Chapter 3. Similar to the leaf orientation angle, the photon scattering angles θ_s and ϕ_s are generally assumed to be independent and therefore separable. Because of the assumed isotropic nature of the BSDF of leaves, the scattering azimuth angle is uniformly random on the interval $[0,2\pi]$. At each scatter a random scattering azimuth angle is selected using the same form as in Equation 3.27.

$$\phi_l = 2\pi x \tag{4.17}$$

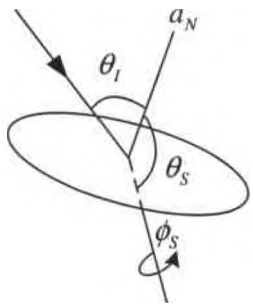

Figure 4.9 Depiction of leaf scattering angle.

There are three different models for the leaf zenith scattering functions which are written into the code: (1) ideal Lambertian, (2) Lambertian-Rayleigh, and (3) the interpolated data method. Each model depends on the incident angle of the incoming

photon, for which an expression is derived in Appendix Five. The ideal Lambertian method assumes the zenith scattering angle pdf to be Lambertian regardless of incident angle. The Lambertian-Rayleigh model assumes the diffuse reflection and transmission to be Lambertian and the specular reflection to be modeled by a reversed Rayleigh distribution. The interpolated data method employs the Rayleigh distribution for specular reflection, but uses the method for interpolating the BSDF explained in section 3.2.5 to model the diffuse reflection and transmission components. After scattering angles from the leaf have been selected, a coordinate transformation must take place to convert from the coordinate system of the individual leaf to that of the overall canopy. Calculations for doing so are found in Appendix Six.

4.5.1 Ideal Lambertian

The ideal Lambertian method for modeling the leaf scattering function is the most basic model. When selecting this model, both the leaf reflection and transmission distribution functions are described by a Lambertian cosine curve. Regardless of the angle of illumination of the leaf, both the BRDF and the BTDF are assumed to be Lambertian. As was derived in section 2.1.5, the random selection of a zenith scattering angle is performed using the equation:

$$\theta_l = \text{asin}(x) \tag{4.18}$$

4.5.2 Lambertian-Rayleigh

The Lambertian-Rayleigh method entails modeling the transmission and the diffuse reflection as Lambertian, while accounting for the specular reflection peak with a

reversed Rayleigh distribution. The expression for generating a reverse Rayleigh distributed random variable θ_S is found by first converting the pdf into the corresponding cumulative distribution function by integration.

$$F_{\theta_S}(\theta_S) = \frac{1}{(90-a)^2} \int_0^{\theta} \theta \exp\left[-\frac{(90-\theta)^2}{2(90-a)^2} \right] d\theta$$

$$F_{\theta_S}(\theta_S) = 1 - \exp\left[-\frac{(90-\theta_S)^2}{2(90-a)^2} \right] \tag{4.19}$$

The relationship between x and θ_S is such that $x = F_{\theta_S}(\theta_S)$, which means that,

$$\theta_S = F_{\theta_S}^{-1}(x)$$

Solving for the inverse of the cdf gives

$$\theta_S = 90 - \text{sqrt}\left[-2(90-a)^2 \ln(1-x) \right]. \tag{4.20}$$

4.5.3 Interpolated Data Model

The third method for scattering from leaves is the interpolated data method. In this model, the specular and diffuse reflection are once again distinguished from each other and given separate distribution functions. The specular reflection is once again modeled by the Rayleigh distribution. The diffuse reflection and transmission functions are interpolated through the method discussed in section 3.2.5. That is, for a given incident angle the transmission and diffuse reflection distribution functions are created. The resulting functions are essentially probability density functions describing the probability of a photon being scattered in each direction. Because there is no analytic expression for the pdf, the relation between a uniformly distributed random variable and the random variable for scattering angle cannot be derived. An alternate method must be used.

The cdf is created by integrating the BTDF and is shown in Figure 4.10. A random value for the variable θ_S is found by taking the absolute value of the difference between the cdf and a random number between 0 and 1 as is done in Figure 4.11. The value of the random variable θ_S is found to be the location where the curve is equal to 0. If x is a uniformly distributed random number between 0 and 1 and $F_{\Theta_s}(\theta_s)$ is the cdf, then the randomly selected scattering angle is found by,

$$\theta_S = \min\left(\left|x - F_{\Theta_s}(\theta_s)\right|\right). \tag{4.21}$$

This model is much slower than the other two, as it requires a new distribution function to be generated for each leaf interaction, but is the most accurate given the measured data.

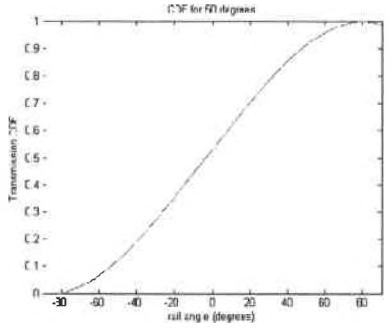

Figure 4.10 Cumulative distribution function for the transmission data at 50 degrees.

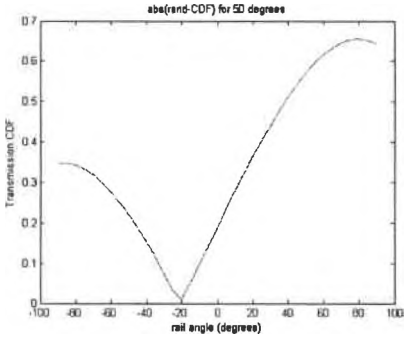

Figure 4.11 Selection of the random variable θ_S.

4.6 Boundary Conditions

After the photon is scattered from a leaf and propagated to the next leaf, the boundary conditions of the canopy must be examined to decide whether another instance of the algorithm must be run. The final spatial location of the photon after each jump is tested.

First, the radial location of the photon is examined. If the photon is located outside the radius of the canopy, then the photon is considered to be side-scattered. The ray is then traced backwards to the edge of the canopy and the spatial, angular and temporal coordinates of the photon are stored. See Appendix Seven for the method of back-tracing the photon to the canopy edge. The second check performed is to see if the photon was backscattered from the canopy without first hitting the ground. If the z-location of the photon is 0, then this is the case. Thirdly, if the photon has experienced over 50 interactions, it is halted as the loss would be A^{50}, which is very small. Lastly, if the photon has exited the canopy by first hitting the ground and then exiting through the top of the canopy, it is considered a good photon. The algorithm is stopped if any of the above conditions are met, and the spatial, angular, and temporal coordinates of the photon are stored. Otherwise, the algorithm is recalled and the canopy propagation continues.

4.7 Final Canopy Propagation Model

The code for the canopy propagation model is written with robustness so that many different canopy parameters may be changed very easily without having to edit the core of the code. Canopy parameters such as canopy height, radius, maximum leaf area

density, corresponding height, etc. are all easily modified. The parameters that describe the canopy modeled in the simulations are given in Table 4.2 below.

The code for the canopy propagation model consists of five files, each of which performs a specific task. CanopyCALC.m is the master file which begins the simulation of each photon and stores the final data to file. The function CanopySCAT.m scatters the photon from leaf to leaf, all the while tracking the spatial and angular locations of the photon. CanopyRegion.m performs the region to region propagation of the photon between interactions. In the case that the interpolated data method is selected, CanopyT.m and CanopyR.m are used to generate the BTDF/BRDF of the leaf for a given incident angle, which are then used to randomly generate the scattering angle from the leaf.

Table 4.2: Final Canopy Propagation Model Parameters

Incident Zenith Angle	0 Degrees
Incident Azimuth Angle	0 Degrees
Incident Photon Location	(0,0,0)
Canopy Height	15 m
Canopy Radius	30 m
LAD_{MAX}	1.45 m^-1
$Height_{LADMAX}$	0.85
Leaf Species	Maple
Leaf Diameter	12.62 cm
# Bins	50
Bin Uniformity	Non-uniform

Chapter 5

Simulation Results

The accuracy of the Monte Carlo method increases as the number of realizations input into the system increases. In accordance with the weak law of large numbers, the mean of the set of realizations approaches the actual statistical average as the number of realizations becomes very large.[12] Thus, in order to obtain an accurate statistical description of the canopy's interaction with the photons the code must be run for a large number of incident photons. Data was collected for approximately 150 million photons incident photons for each model. Such quantities required multiple computers running rather consistently over a period of 3 months to acquire. This quantity gives smooth curves when plotting the probability density functions for returning photons.

The photons returning to the detector are classified in two ways: signal and noise. The signal photons are those that strike the ground while noise photons refer to those that backscatter from the leaves to the detector without hitting the ground. The goal is to maximize the signal and minimize the noise.

5.1 Data Collection

Simulations are run for each of the three leaf scattering models in order to compare the efficiency and accuracy of each. Seeing as the interpolated data model uses the actual BSDFs we measured from real leaves, it will be taken to be the standard of accuracy to which the other two models will be judged. Preliminary results showed that the interpolated data model is the least efficient in terms of run time. The code for this model takes approximately 5 times as long to run as the other two. Therefore, if either the ideal Lambertian or the Lambertian-Rayleigh models exhibit similar results to the interpolated data model, they may be a more desirable method of modeling the leaf scattering distribution.

We will examine the spatial, angular and temporal probability density functions of photons in two planes of interest of the canopy; the first being the ground plane. Spatial locations of photons in the ground plane are of interest for the purpose of imaging a target on the ground. If the photon does not hit within a specific region on the ground it can be classified as noise and has an adverse effect on imaging. The other plane of interest is the plane of a sensor located 50 meters above the canopy. Once the photons reach the top of the canopy they no longer interact with any leaves, and propagate through free space in the direction from which they left the canopy. Located 50 meters above the canopy is the lens plane, in which a lens is used to focus the photons onto a detector. The simulations use two different lenses. The first has a diameter of 10 cm and a focal length of 20 cm. The second lens has a diameter of 25 cm and a focal length of 50 cm, giving both lenses an f-number of 2.

5.1.1 Ideal Lambertian Data

A telling statistic of each model is the fraction of incident photons that are absorbed, side scattered, back scattered, and signal. For the ideal Lambertian model, the fraction of absorbed photons is 16.457%; the fraction of side scattered photons is 12.9198%; the fraction of backscattered photons is 66.294%; and the fraction of signal photons is 4.5656%. It might be alarming that only 6.5656 percent of the incident photons actually make it to the top of the canopy after striking the ground. Furthermore, this number is a very high-end estimate as it considers all photons which exit the canopy regardless of location. Obviously photons that leave the canopy at the very edge of the radius (30 meters from the detector) are of no interest, as they will not be detected. A better tell of the result of the simulation are the probability density functions of the spatial, temporal, and angular locations of the photons.

Figure 5.1 contains the probability density functions for the x and y locations of where the photons arrive on the ground. Notice the Gaussian-like shape of the two curves. This is expected, as the sum of a number of statistically independent random variables is itself distributed in a Gaussian manner, per the central limit theorem.[12] The peak is located at 0 meters and the FWHM is approximately 20m for both the x and the y pdfs, which means most of the photons arrive where they were targeted. The two functions go to zero at the radial boundary of the canopy, rather than tending to zero at +/- infinity (as is the case with an ideal Gaussian curve) because of the constraints on the radius of the canopy. Whenever a photon leaves the radius of the canopy it is considered side scattered and its propagation is terminated. So all the photons that would have struck the ground at x and y locations greater than the radius of the canopy (30 meters) are not

included in this plot. Therefore the tail ends of the curve go to zero at 30 meters rather than +/- infinity.

Another thing worth noting is that the process of a photon scattering from leaf to leaf through the canopy is a combination of many random processes. The average number of times a photon interacts with a leaf in the canopy is 20.4328. This brings up an important theorem in random variables: the central limit theorem. The central limit theorem states that any sum of many independent, identically distributed random variables will tend to be distributed according to normal distribution. That is, the sum of a large number of random processes, regardless of the individual distributions, results in a final Gaussian-like distribution.[12]

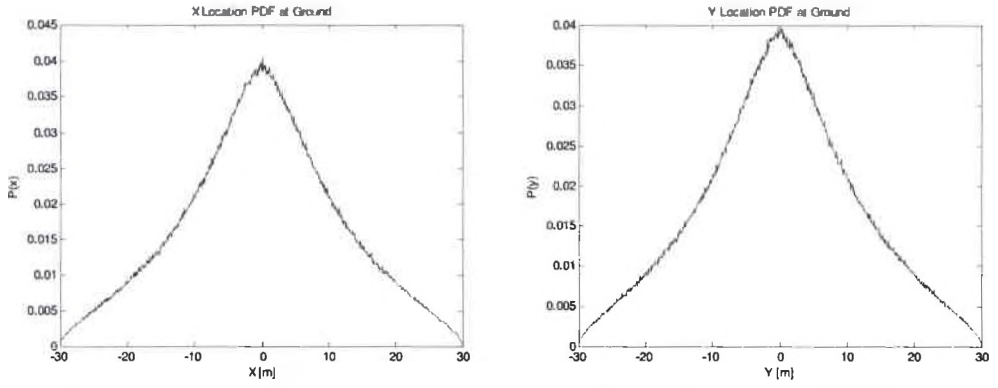

Figure 5.1 Probability density functions for the x- and y-location of the photons on the ground.

The radial location is then found by the expression $r = \sqrt{x^2 + y^2}$ and plotted in Figure 5.2 (blue curve). Note that this radial pdf has unequal bin area. As the radius increases, so too does the bin area as the square of the radius: $A = \pi\left(r_2^2 - r_1^2\right)$. It is difficult to gather information from this plot. Looking only at the radial pdf, one would think that there is a donut shaped illumination on the ground with a hole at the center. A

better unit of measure is made by dividing each bin in the radial location pdf by the bin area, thus giving a good representation of photons intensity on the ground as a function of radius, rather than the photon number. Also shown in Figure 5.2 is a semi log plot of the radial intensity (green curve) which is plotted linearly against the radius. The radial intensity plot gives a much better representation of the ground illumination profile. Note that most of the photons hit the ground near the zero radius, and the intensity tails off towards zero as the radius increases.

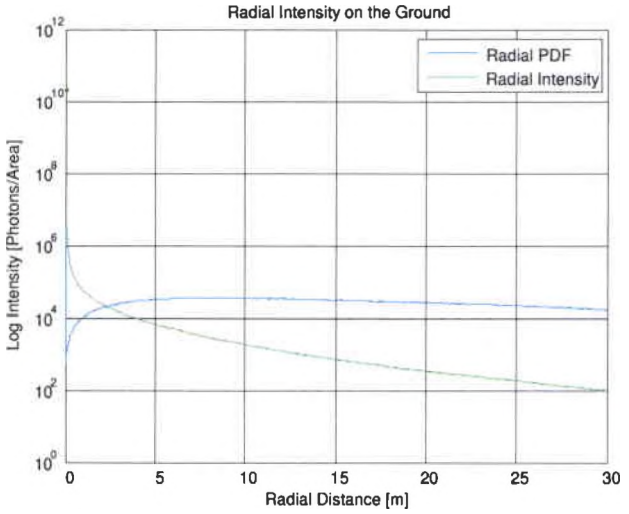

Figure 5.2 Radial intensity and radial location pdf of the photons on the ground for the ideal Lambertian model.

The plot of the intensity as a function of radius for the photons in the plane of a lens located 50 meters above the canopy is given in Figure 5.3. Note that this plot looks very similar in shape to the plot of the intensity of photons in the ground. However, the two plots differ in magnitude. The intensity of photons in the lens plane is much more spread out than in the ground plane. There is more photon intensity in the outer regions of the radius in the lens plane than on the ground as would be expected. As the photons propagate through free space they spatially spread, since they are nominally angularly

diverging from the canopy center (which is seen in the zenith angle pdf shown in Figure 5.4(b)). Still, most of the photons are located at the zero radius location. Also, note that the lens plane intensity includes all photons that reach the lens plane, regardless of whether they are backscattered or if they hit the ground.

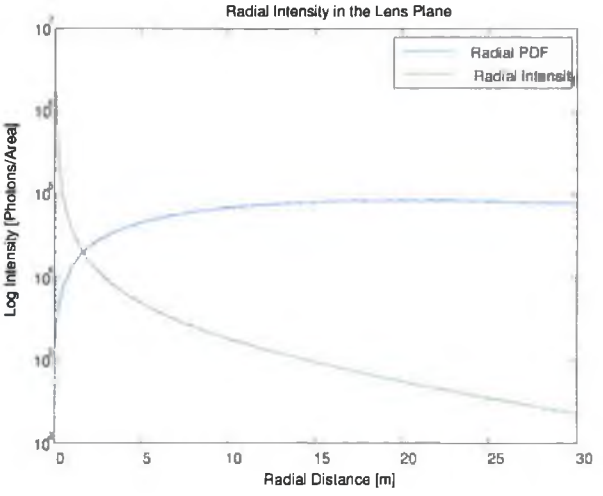

Figure 5.3 Radial intensity and radial location pdf of the photons in the lens plane for the ideal Lambertian model.

The angular pdfs also aid in describing what happens to the photons in the canopy. Plotted in Figure 5.4(a) is the azimuth angle pdf. As expected, the propagation model shows no preference to azimuth orientation. The curve is flat across 0 to 2π. The zenith angle pdf is plotted in Figure 5.4(b). Almost none of the incident photons return to the top of the canopy (or the lens) with 0 degrees incidence. Most of the photons are deflected from their initial path. The zenith angle pdf is not Gaussian shaped because it is not a sum of independent random processes. The final angle of exit of the photons is dependent only upon the scattering angle from the final leaf. Any interactions that happen before this final leaf are of no consequence. Therefore, the zenith angle pdf would look

the same regardless of the thickness of the canopy or the number of scattering events within the canopy.

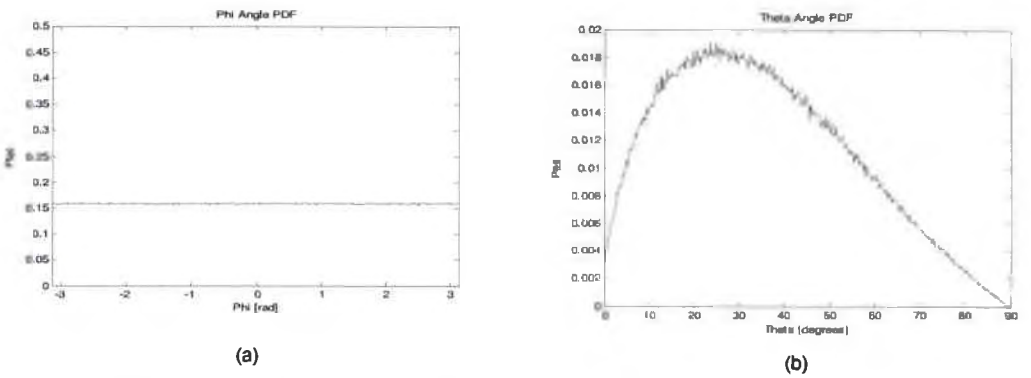

Figure 5.4 The (a) azimuth and (b) zenith angle pdfs for the ideal Lambertian model.

The final dimension of interest is temporal. The transit time pdf of the photons through the canopy is plotted in Figure 5.5. The blue curve represents that pdf of *all* the photons which arrive in the lens plane, and the red curve represents only the signal photons which arrive in the lens plane. Most of the noise photons make it back to the lens plane before any of the signal photons begin to arrive. This makes intuitive sense, because the signal photons have to travel all the way to the ground and back where the noise photons need only to travel a fraction of that distance, as they are reflected backwards to the top of the canopy before striking the ground. The distributions are Rayleigh-shaped, which also flows naturally because there will be a few early photons and many photons which can be trapped in the canopy for quite some time before making it back out.

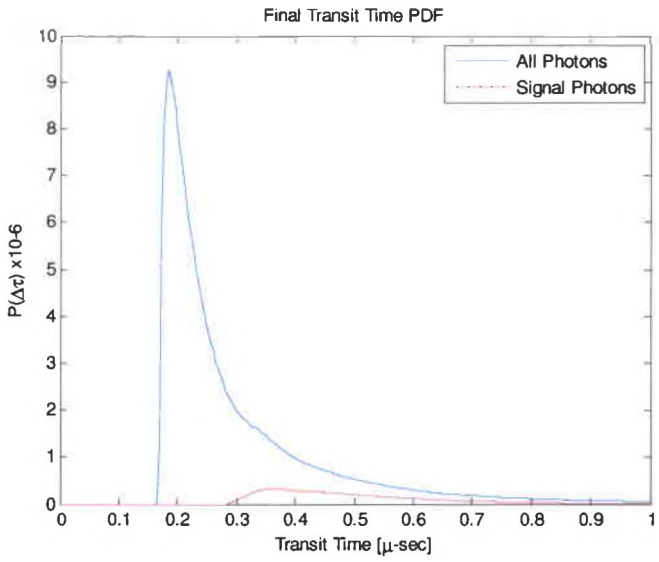

Figure 5.5 Temporal pdf (ideal Lambertian model) of the signal photons and all the photons which make it back to the lens plane.

However, knowing only the arrival time pdf on the detector says nothing about where the photons arrive in the plane. Similarly, knowing only where the photons arrive gives no information about when they arrive. The two dimensions are intertwined such that photons that bounce around in the canopy have long transit times, and are generally spatially dispersed in the lens plane. Similarly, photons that do not encounter very many interactions do not spatially spread very much nor do they have high transit times. It is important to look at the temporal and spatial domain at the same time. Plotted in Figure 5.6 is the spatio-temporal scatter plot of the arrival times/locations of the photons onto a detector after focusing by a 10 cm diameter, 20 cm focal length lens. Plotted in Figure 5.7 is the same plot using a 25 cm diameter, 50 cm focal length lens.

Each dot in the figure represents a single photon. The blue dots correspond to the noise photons and the red dots to the signal photons. Plotted along the horizontal-axis is the radial location (in meters) of the arriving photons. Along the vertical axis is the

arrival time of the photon. Knowledge of when and where the individual photons are arriving on the detector is gathered from this plot. Notice that the noise photons arrive, on average, about 0.1 micro-seconds before the signal photons arrive on the detector. It appears that range gating may be performed on the detector to filter out the noise photons.

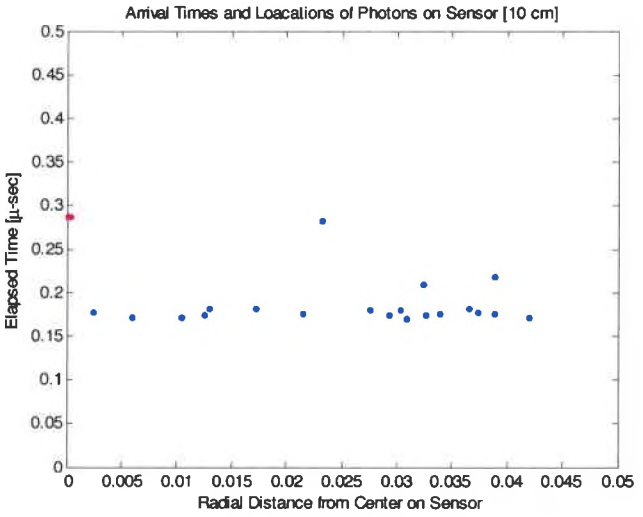

Figure 5.6 Spatio-temporal arrival of photons onto a detector using a 10 cm diameter, 20 cm focal length lens. Ideal Lambertian model.

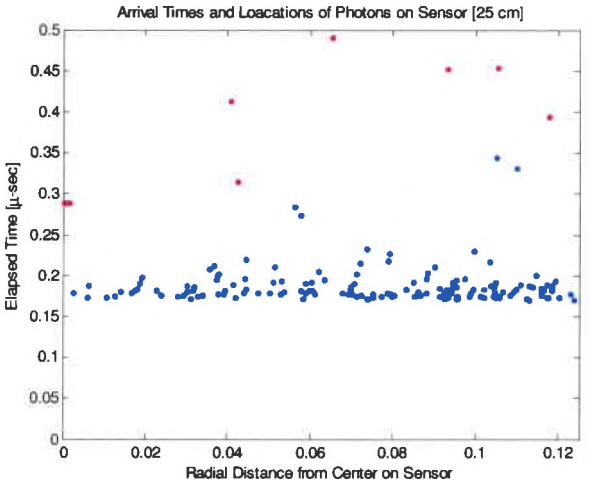

Figure 5.7 Spatio-temporal arrival of photons onto a detector using a 25 cm diameter, 50 cm focal length lens. Ideal Lambertian model.

5.1.2 Lambertian-Rayleigh Data

The data collected from the Lambertian-Rayleigh model is very comparable to that of the ideal Lambertian model. The fraction of absorbed photons is 15.631%; the fraction of side scattered photons is 13.683%; the fraction of backscattered photons is 66.358%; and the fraction of good signal photons is 4.0904. Intuitively one may think that including the glint from the leaf would increase the amount of side scattering dramatically, but this is not the case. The fraction of photons that are side scattered is a little higher for the Lambertian-Rayleigh model, but not significantly. This might be due to the fact that the leaves are randomly oriented in the canopy, so the glint angle does not necessarily always point outwards towards the side.

The x- and y- ground location pdfs for the Lambertian Rayleigh model are essentially identical to those of the ideal Lambertian model (Gaussian-like centered at 0, FWHM ~ 20 meters), as seen in Figure 5.8. The radial intensity of photons on the ground is plotted in Figure 5.9. Once again the intensity of photons is greatest at the center of the canopy and drops off as the radius increases. The intensity of photons is slightly lower near 0m radius for this version of the code than it was for the ideal Lambertian model, but not significantly. The angular pdfs are very similar to those found from the ideal Lambertian data, as seen in Figure 5.10. There is a small difference in the zenith angle pdf, which can be attributed to the addition of the specular reflection peak. Similarly, the temporal pdf is nearly identical to the ideal Lambertian case. See Figure 5.11. Similar results are seen in the spatio-temporal plots (see Figures 5.12 and 5.13 for 10cm and 25cm diameter lenses, respectively) where the noise photons arrive first onto the detector and then the signal photons arrive about 0.1 microseconds later.

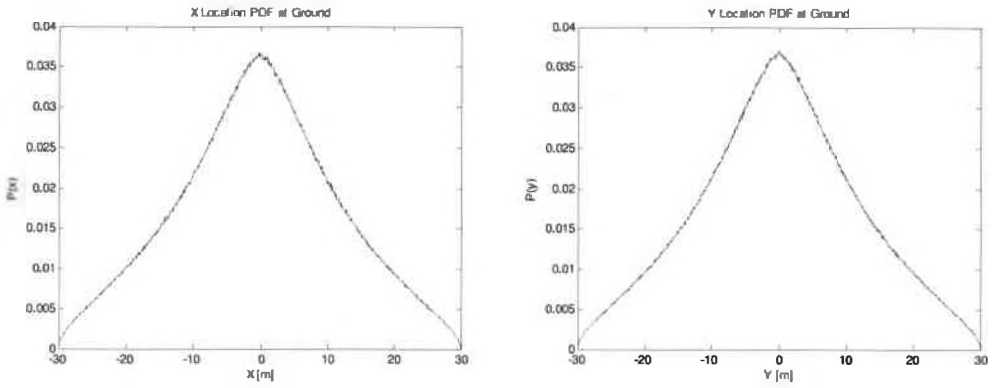

Figure 5.8 Probability density functions for the x- and y-location of the photons on the ground.

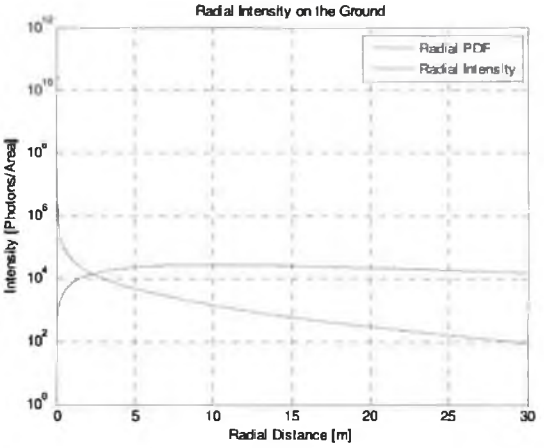

Figure 5.9 Radial intensity and radial location pdf of the photons on the ground for the Lambertian-Rayleigh model.

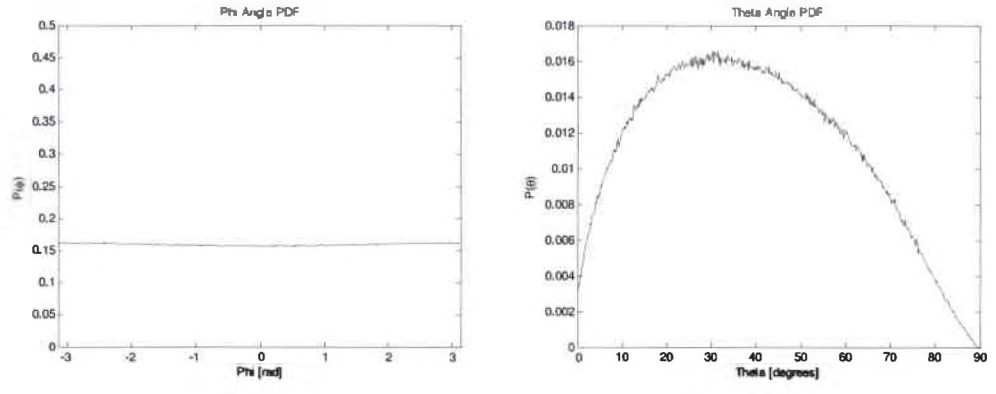

Figure 5.10 The (a) azimuth and (b) zenith angle pdfs for the Lambertian-Rayleigh model.

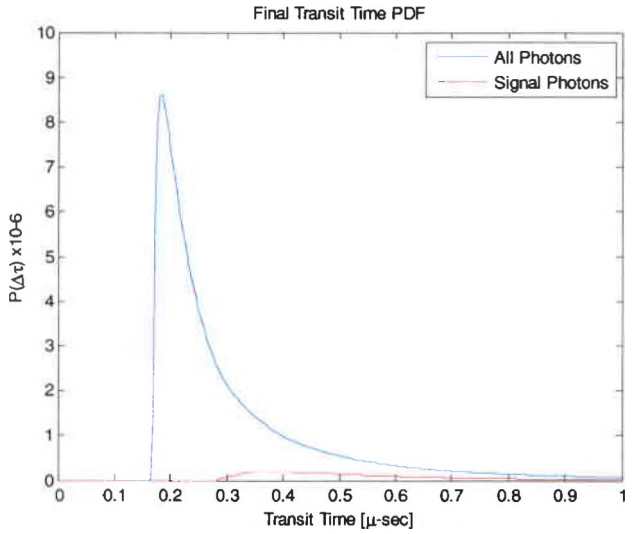

Figure 5.11 Temporal pdf (Lambertian rayleigh model) of the signal photons and all the photons which make it back to the lens plane.

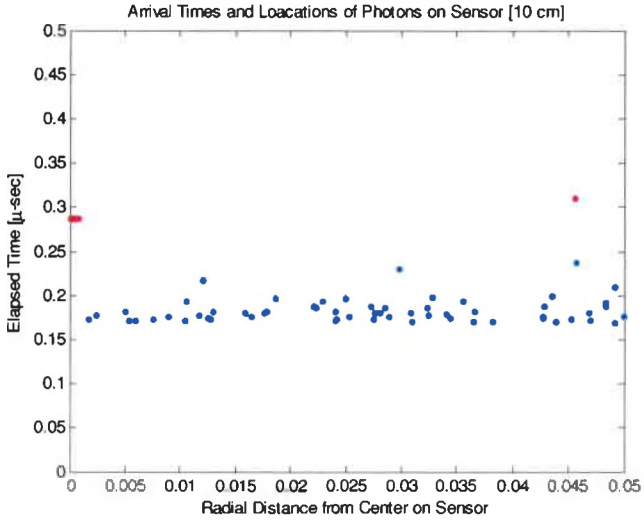

Figure 5.12 Spatio-temporal arrival of photons onto a detector using a 10 cm diameter, 20 cm focal length lens. Lambertian-Rayleigh model.

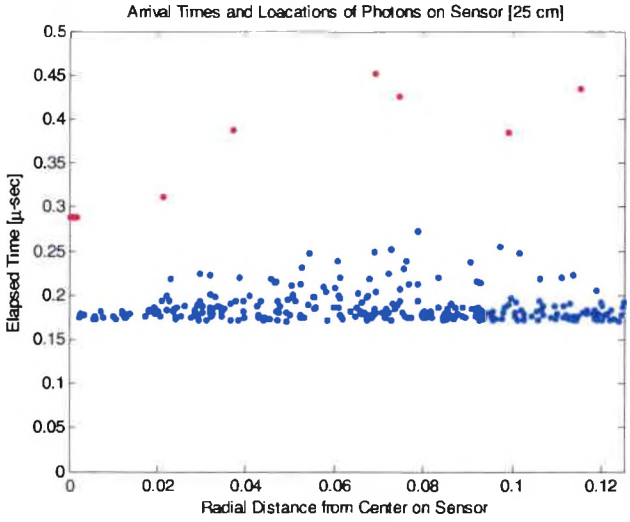

Figure 5.13 Spatio-temporal arrival of photons onto a detector using a 25 cm diameter, 50 cm focal length lens. Lambertian-Rayleigh model.

5.1.3 Interpolated Data

For the interpolated data model, the fraction of absorbed photons is 15.72%; the fraction of side scattered photons is 14.11%; the fraction of backscattered photons is 65.88%; and the fraction of good signal photons is 4.287%. Once again, the fraction of side scattered photons is a little higher than in the other two models, but not significantly. In fact, the photon has about the same probability of being side scattered/back scattered/absorbed in each of the three models. There are minor differences, but none to any significant magnitude.

The probability density functions for the interpolated data method are very similar in shape and magnitude to those of the other two models, as can be seen in Figures 5.14 through 5.19. The pdfs of radial intensity on the ground and radial intensity at the lens plane are nearly identical to the previous pdfs we have seen. Once again, near-Gaussian curves are centered about 0 with a FWHM of approximately 20m.

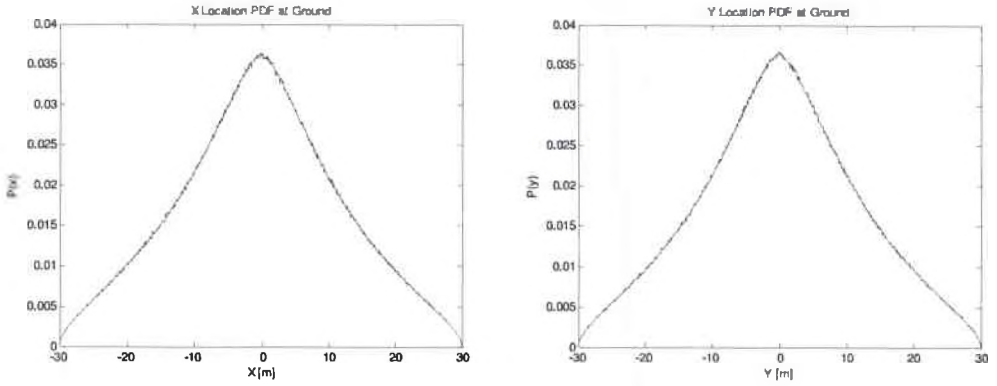

Figure 5.14 Probability density functions for the x- and y-location of the photons on the ground.

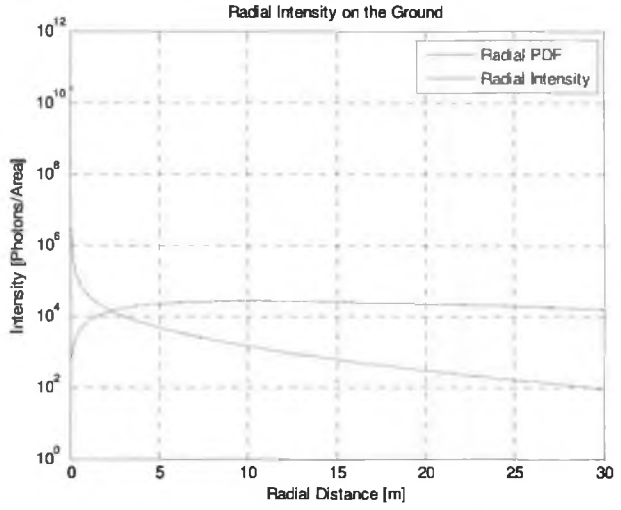

Figure 5.15 Radial intensity and radial location pdf of the photons on the ground for the interpolated data model..

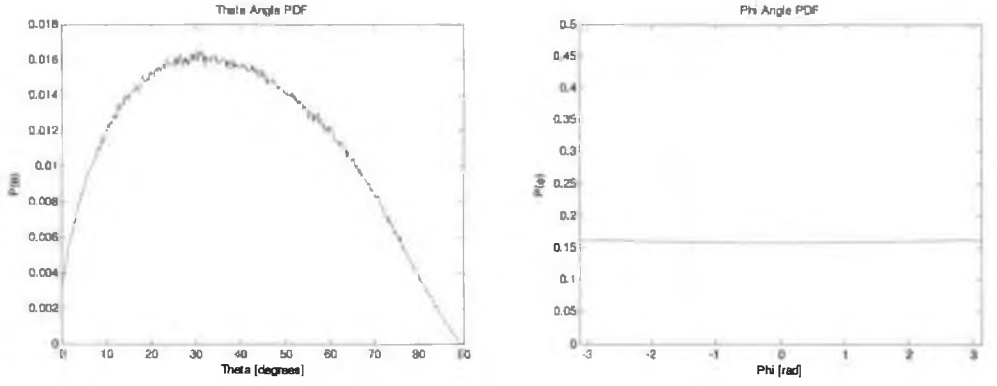

Figure 5.16 The (a) azimuth and (b) zenith angle pdfs for the interpolated data model.

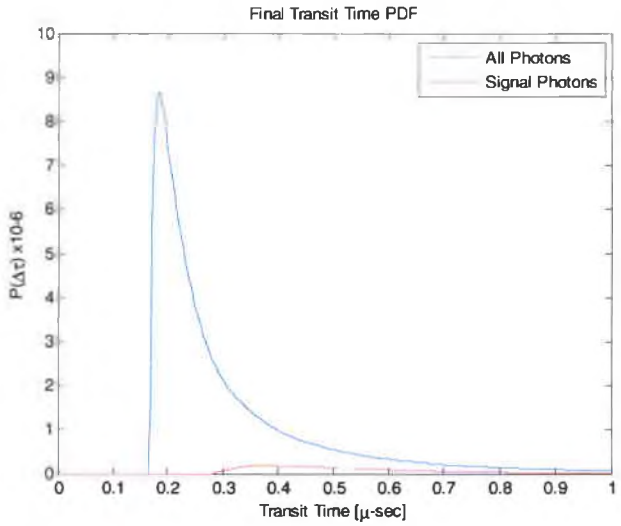

Figure 5.17 Transit time pdf of the signal and noise photons which make it back to the lens plane.

The spatio-temporal scatter plot remains the same, as the low-end boundary of arriving transit times is not affected. The first photons still arrive at the same time independent of when the latest arriving photons reach the lens plane. All of the noise photons arrive on the detector before any of the signal photons return.

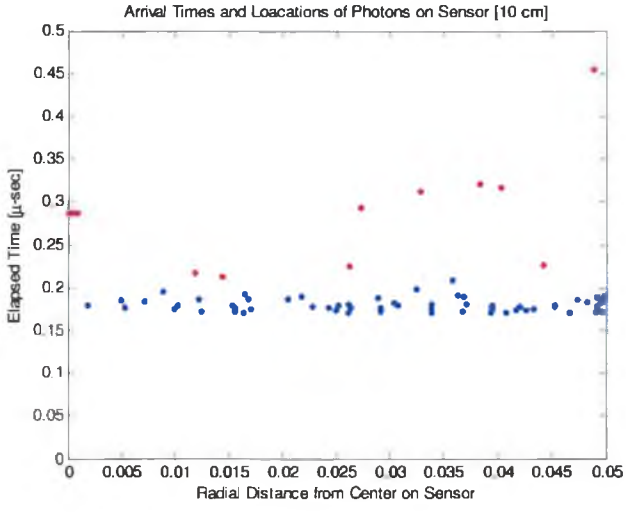

Figure 5.18 Spatio-temporal arrival of photons onto a detector using a 10 cm diameter, 20 cm focal length lens. Interpolated data model.

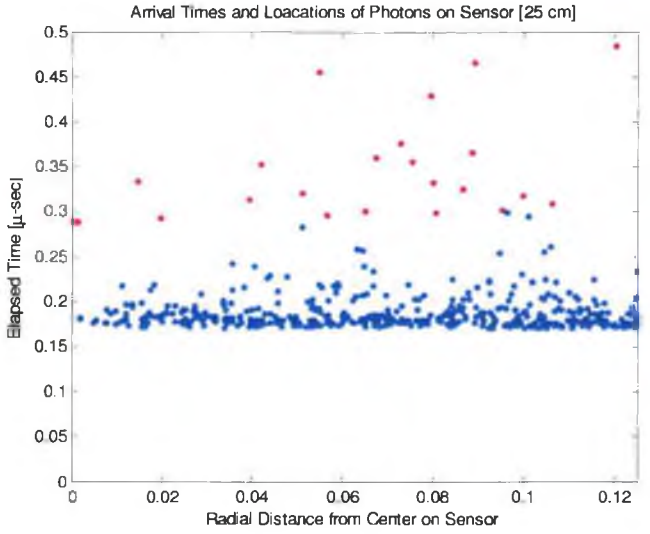

Figure 5.19 Spatio-temporal arrival of photons onto a detector using a 25 cm diameter, 50 cm focal length lens. Interpolated data model.

5.1.4 Comparison of Models

Upon comparing the results of all three models, it becomes apparent that the method for modeling the scattering of light from the individual leaves does not have much of an effect on the final outcome of the propagation. Because each photon experiences about 20 interactions on average, the pdfs of the statistically independent individual scatterers have minimal effect. In light of the central limit theorem, the final radial location of the photons is not surprisingly Gaussian for all three models. Similarly, the arrival times of the photons on the detector do not vary much from model to model. It can be conclusively said that the diffuse scattering model an individual leaf is of little consequence on the outcome of the simulation. Therefore, it will be best to use the Lambertian-Rayleigh case for any further simulations. Data acquired using this model matches the data acquired using the measured BSDFs almost exactly.

In addition, there may be some concern that only 150 million photons have been simulated through the canopy and there are only tens of photons returning to the detector. However, consider the fact that a single 100mJ pulse from a 1064nm laser contains about 5.3629×10^{17} photons per pulse.

$$\lambda = 1064\text{nm}$$

$$E_\lambda = \frac{hc}{\lambda} = 1.1654\text{eV} = 1.8647\times10^{-19}\text{J}$$

$$E_p = 0.1\text{J}$$

$$\text{Photons Per Pulse} = \frac{E_p}{E_\lambda} = 5.3629\times10^{17}$$

The total number of incident photons that have been simulated is not even comparable to the actual number of photons contained in a typical single pulse. One would multiply the current number of returning photons by an order of magnitude of 10^8 to achieve a realistic response.

5.1.5 Signal-to-Noise Ratio

It is important that a signal-to-noise ratio of at least 1 is obtained. If an SNR of 1 is not reached, the signal will not be discernable from the noise in the system. The optical signal power that gives such a SNR is known as the receiver sensitivity. There are several sources of noise which are inherent to the detection process: shot noise, thermal noise, dark current, and background photons. The thermal noise and dark current are function of the detector, and constant in terms of the number of detected photons. Shot noise and background noise, however, rely heavily on the number of photons collected by the detector.

The signal-to-noise ratio goes as the inverse of the background noise term, which means that our SNR goes down as the number of detected background photons goes up. It is therefore very desirable to minimize these background photons. One method for doing so is to range gate the detector so that it only detects photons for a specific period of time. According to the temporal pdfs presented earlier in this chapter, the great majority of noise photons exited the canopy a few microseconds before any of the signal photons. Moreover, after propagating all the photons to a 25cm diameter detector located 50m above the canopy, the arrival times of the noise and signal photons is even more segregated as shown in Figure 5.20. Almost all of the noise photons return before any of the signal photons. We can zoom in on the region where the signal photons first begin to arrive for a better look at the possibility of range gating, as is done in Figure 5.21. Using the detector to integrate over the range from $0.28390\,\mu s$ to $1\,\mu s$, we can effectively minimize the detected noise. Also note, this is intended to be a worst case scenario so we have not plotted the ballistic photons.

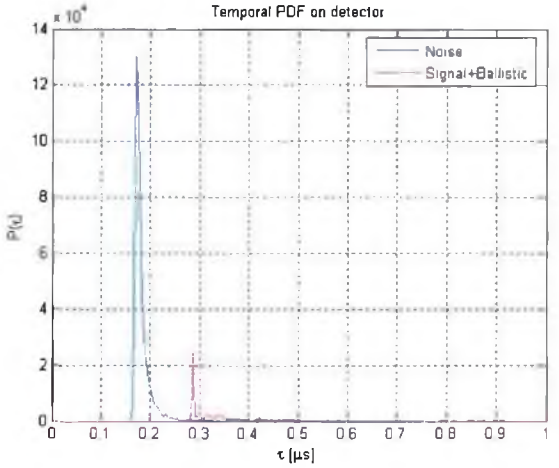

Figure 5.20 Temporal pdf of signal (red) and noise (blue) photons returning to a 25cm diameter pupil located 50m above the canopy.

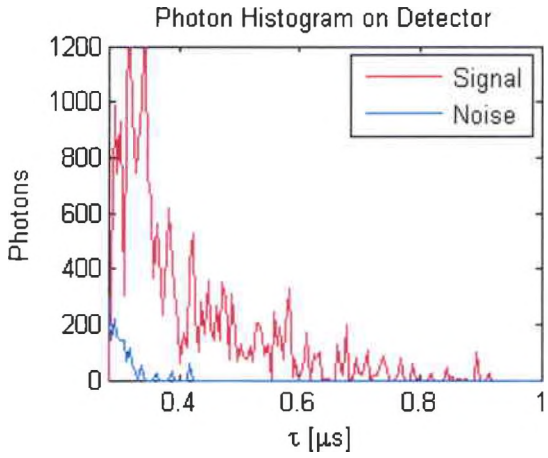

Figure 5.21 Histogram of the number of photons arriving within certain time bins on the detector.

Using range gating and several parameters which describe typical pulsed lasers and InGaAs PIN photodiodes we will calculate the expected SNR and the receiver sensitivity for a single laser pulse propagating through our canopy. If we assume a rectangular pulse train of pulse width 1ns and pulse repetition rate 5kHz, the integration time of the detector will be much less than the spacing between pulses, as can be seen in Figure 5.22. The rectangular pulses are the inputs to the system. At some time later the broadened signal (red) and noise (blue) pulses return to the detector. Because the spacing between the successive pulses is so much greater than the integration time of the detector, there will be no issues with the returning, broadened pulses overlapping.

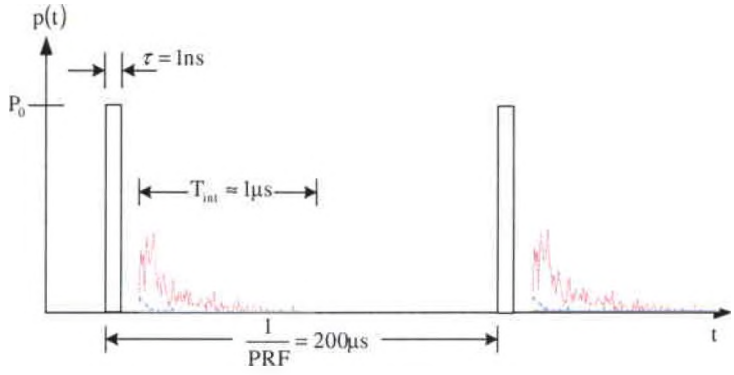

Figure 5.22 The detector integration time is less than the spacing between the successive pulses.

The SNR can be calculated then from these noise sources according to the equation,

$$\mathrm{SNR} = \frac{\left\langle i_{\mathrm{signal}}^2 \right\rangle}{\left\langle i_{\mathrm{shot}}^2 \right\rangle + \left\langle i_{\mathrm{thermal}}^2 \right\rangle + \left\langle i_{\mathrm{dark\ currents}}^2 \right\rangle + \left\langle i_{\mathrm{background}}^2 \right\rangle}. \tag{5.1}$$

This equation can be rewritten in terms of the power of the detected photons and detector responsivity, R, according to the following relation,

$$\mathrm{SNR} = \frac{R^2 \left\langle P_s^2(t) \right\rangle}{2qB\left(I_D + R\left\langle P_t(t) \right\rangle\right) + R^2 \left\langle P_n^2(t) \right\rangle + \dfrac{4k_B TB}{R_L}}, \tag{5.2}$$

where $P_s(t)$ is the instantaneous detected optical signal power, $P_n(t)$ is the instantaneous background optical noise power, and $P_t(t)$ is the instantaneous total detected optical power (noise + signal).

The instantaneous signal power can be calculated from the number of signal photons, $N_s(t)$, arriving in each time bin of our histogram from the equation,

$$\mathrm{P}_s(t) = \frac{h\nu}{\Delta\tau} N_s(t). \tag{5.3}$$

The mean-squared optical signal power can be found by integrating this expression over the duration of the returning pulse,

$$\left\langle \mathrm{P}_s^2(t) \right\rangle = \frac{1}{\mathrm{T_{int}}} \int_{t_0}^{t_0+\mathrm{T_{int}}} P_s^2(t)\,dt, \tag{5.4}$$

where t_0 is the beginning of the pulse and T_{int} is the signal pulse duration. We can approximate this value by converting the integral into a summation over the number of bins in our histogram, M,

$$\left\langle P_s^2(t)\right\rangle \approx \frac{1}{T_{int}}\sum_{i=1}^{M}\frac{(h\nu)^2 N_{s,i}^2}{\Delta\tau^2}\Delta\tau. \tag{5.5}$$

After simplification, the mean-squared optical signal power can be expressed as,

$$\left\langle P_s^2(t)\right\rangle \approx \frac{(h\nu)^2}{T_{int}\Delta\tau}\sum_{i=1}^{M}N_{s,i}^2. \tag{5.6}$$

Similarly, the mean-squared optical background power can be expressed by summing the number of background noise photons arriving instantaneously in each time bin,

$$\left\langle P_n^2(t)\right\rangle \approx \frac{(h\nu)^2}{T_{int}\Delta\tau}\sum_{i=1}^{M}N_{n,i}^2, \tag{5.7}$$

Where N_n is the number of backscattered noise photons returning to the detector. The mean total detected power can also be approximated by summing the instantaneous total power,

$$\left\langle P_t(t)\right\rangle \approx \frac{1}{T_{int}}\sum_{i=1}^{M}\frac{h\nu(N_{s,i}+N_{n,i})}{\Delta\tau}\Delta\tau. \tag{5.8}$$

After simplification, the expression becomes,

$$\left\langle P_t(t)\right\rangle \approx \frac{h\nu}{T_{int}}\sum_{i=1}^{M}(N_{s,i}+N_{n,i}). \tag{5.9}$$

Inserting Equations 5.6, 5.7, and 5.9 back into Equation 5.2 gives us an expression for calculating the signal-to-noise ratio of a single pulse in terms of the numbers of detected signal and background noise photons and several known laser/detector parameters,

$$SNR = \frac{\frac{(\eta q)^2}{T_{int}\Delta\tau}\sum_{i=1}^{M}N_{s,i}^2}{2qB\left(I_D+\frac{\eta q}{T_{int}}\sum_{i=1}^{M}(N_{s,i}+N_{n,i})\right)+\frac{(\eta q)^2}{T_{int}\Delta\tau}\sum_{i=1}^{M}N_{n,i}^2+\frac{4k_BTB}{R_L}}. \tag{5.10}$$

Also note that the responsivity, R, has been replaced with $\frac{\eta q}{h\nu}$ for simplification.

Recall, that the number of photons we have simulated through the canopy is not even comparable to the total number of photons contained in a single pulse. However, in order to get a useful result we need to use values that would be on the order of what we would expect for a typical laser pulse. Therefore, we must scale the number of signal and noise photons we have collected in each bin by a factor, α, such that α is the ratio of the typical number of photons per pulse to the total number of photons we have sent into the canopy thus far. As calculated in the previous section, the typical number of photons in a real 100mJ pulse is 5.3629e+17. We have simulated the propagation of 2.9739e+010 photons through the canopy, which gives an α value of 1.8033e+007. Equation 5.10 can then be rewritten to include this term,

$$\mathrm{SNR} = \frac{\frac{(\eta q)^2}{\mathrm{T_{int}}\Delta\tau}\alpha^2\sum_{i=1}^{M}N_{s,i}^2}{2qB\left(I_D + \frac{\eta q}{\mathrm{T_{int}}}\alpha\sum_{i=1}^{M}\left(N_{s,i}+N_{n,i}\right)\right) + \frac{(\eta q)^2}{\mathrm{T_{int}}\Delta\tau}\alpha^2\sum_{i=1}^{M}N_{n,i}^2 + \frac{4k_BTB}{R_L}} \quad (5.11)$$

Consider, now, an InGaAs PIN photodiode which has the following parameters at a wavelength of 1064nm: $I_D = 1\mathrm{nA}$, $\eta = 0.90$, and $R_L = 1000\Omega$. Assuming $\mathrm{T_{int}} = 0.28390\mu\mathrm{s}$ and $\mathrm{B} = \frac{\mathrm{PRF}}{2} = 2500\mathrm{Hz}$, the signal-to-noise ratio achieved from our simulations for a 25cm diameter detector is 68.5, or 18.3563 dB. This represents a signal level well above the noise.

It can also be found that the receiver sensitivity is reached with an alpha value of 0.0384, which corresponds to1.27×10^9 launched photons. This is also equivalent to a 0.23736nJ pulse.

Chapter 6

Conclusions

It was the goals of this research (1) to quantify and characterize the optical properties of leaves for 1.06 μm laser light and (2) to quantify the temporal, spatial, and angular dispersion experienced by an incident pencil beam through a foliated forest canopy. The results of our work have shown a strong correlation between the scattering properties of maple and cottonwood leaves and the Lambertian distribution function, except when the illumination angle increases past 50 degrees. Beyond this angle, a specular reflection peak emerges and the Lambertian model breaks down, resulting in the need for a new method to model the BRDF of these leaf species. The method implemented in this work not only accurately describes the measured BSDFs, but also allows the interpolation of BSDF values for intermediate illumination and detection angles. Our results will prove to be a valuable tool to other researchers investigating remote sensing applications where the interaction of laser beams and tree leaves must be considered. This work will also aid further studies which may be performed using out-of-plane measurements where the detectors do not lie in the plane containing the surface normal of the leaf and the incident laser beam.

Modeling the bidirectional scattering distribution functions of individual leaves as Lambertian may not be accurate, but in the application of propagating light through a canopy of randomly oriented scatterers, all models converge to the same results. Virtually no difference was seen in the results of the simulations when one model of BSDF was interchanged with another. One can therefore not only conclude that the describing the leaf BSDF as Lambertian is an accurate assumption in this utility, but also that it is the optimal assumption. Selecting random scattering angles according to the Lambertian pdf is not only the easiest to implement, but also the fastest by a factor of nearly 5x.

It is also seen from the results of the simulations that there may be an opportunity for range gating to filter out the unwanted noise photons. Backscattered noise photons appear to arrive on the detector approximately 0.1 microseconds before any signal photons. As the only inputs to the system thus far have been a pencil beam illuminating the canopy at 0 degrees zenith, there is plenty of room for continued research. Further experiments will be to validate the model with experimental data collected from actually illuminating a forest. The gap fraction of a defoliated forest may also be applied to this research to add the element of branches into the model.

References

[1] B. Lalic and D. T. Mihailovic, "An empirical relation describing leaf-area density inside the forest for environmental modeling," American Meteorological Society **43**, 641-645 (2004).

[2] C. Ruiz, P. Borderies, I. Chenerie, E. Mougin, and C. Proisy, "Modeling of electromagnetic waves interaction with forest canopies," CEOS Committee on Earth Observation Satellites (2000).

[3] G. Sun and J. Ranson, "Modeling LIDAR returns from forest canopies," IEEE Geoscience and Remote Sensing **38**, 2617-2626 (2000).

[4] 1Lt. P. Muller, L. Barnes, and M. Dierking, "See Through Leaves," AFRL/SNJM

[5] S. Jacquemoud and S. Ustin, "Leaf optical properties: a state of the art," Proc. 8th International Symposium Physical Measurements & Signatures in Remote Sensing, Aussois (France) CNES, 223-232 (2001).

[6] www.regentinstruments.com Copyright © 1998-2006 by Regent Instruments Inc. for entire contents. (2006).

[7] K. C. McDonald, M. C. Dobson, and F. T. Ulaby, "Modeling multi-frequency diurnal backscatter from a walnut orchard," IEEE, 1125-1128 (1991)

[8] M. A. Karam and A. K. Fung, "A canopy scattering model and its application to a deciduous forest," IEEE, 137-140 (2000)

[9] F.T. Ulaby, K. C. McDonald, K, Sarabandi, M. Whitt, and M. C. Dobson, "Michigan Microwave Canopy Scattering Model (MIMICS)," Proc. IGARSS '88 (Edingburgh, UK) p1009 (1988)

[10] T. Brakke, "Goniometric measurements of light scattered in the principal plane from leaves," IEEE Geoscience and Remote Sensing, 508-510 (1992)

[11] T. Brakke, ""Specular and diffuse components of radiation scattered by leaves," Agr. For Meteorol. **71** 283-295 (1994)

[12] R. Ziemer, *Elements of Engineering Probability & Statistics*, (Upper Saddle River, NJ: Prentice Hall Inc., 1997) pp 45-81

[13] S. Miller and D. Childers, *Probability and Random Processes*, (London: Elseiver Inc., 2004) pp 187-189.

[14] J. Goodman, *Statistical Optics*, (New York: John Wiley & Sons, Inc., 1985) pp 7-59.

[15] K. C. McDonald, M. C. Dobson, and F.T. Ulaby, "Using MIMICS to model L-band mulitangle and multitemporal backscatter from a walnut orchard," IEEE Transactions on Geoscience and Remote Sensing **28**, 477-491 (1990)

[16] E. A. Bucher, "Computer simulation of light pulse propagation for communication through thick clouds," Applied Optics **12**, issue no. 10, 2391-2400 (1973)

[17] P. Lewis and P. Saich, "Radiative transfer theory at optical and microwave wavelengths applied to vegetation canopies," RSU Dept. Geography, University College London, http://www.geog.ucl.ac.uk/~plewis/vegsci2002/, (2002).

[18] H. T. Chuah and H. S. Tan, "A monte carlo method for radar backscatter gtom a half-space random medium," IEEE Transactions on Geoscience and Remote Sensing, **27**, 86-93 (1989).

[19] D. Collins, W. Blattner, M. Wells, and H. Horak, "Backward Monte Carlo calculations of the polarization characteristics of the radiation emerging from spherical-shell atmospheres," Applied Optics **11**, 2684-2696 (1972).

[20] Y. Govaerts and M. Verstraete, "Modeling the scattering of light in three-dimensional canopies: contribution of a Monte Carlo ray tracing approach," Institute for Remote Sensing Applications, 31-34.

[21] H. Jensen, S. Marschner, M. Levoy, and P. Hanrahan, "A practical model for subsurface light transport," International Conference on Computer Graphics and Interactive Techniques, 511-518

[22] D. Falster and M. Westoby, "Leaf size and angle vary widely across species: what consequences for light interception?," New Phytologist **158**, 509-525 (2003)

[23] P. Liang and L. Pierce, "Application of bistatic MIMICS to forest canopies," IEEE, 4328-4331 (2004)

[24] P. Liang, M. Moghaddam, and L. Pierce, "Backscattering simulation for nonuniform forest canopies using multi-layer MIMICS," IEEE 1021-1024 (2004)

[25] M. O. Kolawole, "Radar backscatter model of a defoliated forest using log-periodic antenna array technology," IEEE, 363-368 (1996)

[26] Yvo L. C. de Jong and Matti H. A. J. Herben, "A tree-scattering model for improved propagation prediction in urban microcells," IEEE Transactions on Vehicular Technology **53**, 503-513 (2004)

[27] J. Ross, V. Ross, and A. Koppel, "Estimation of leaf area and its vertical distribution during growth period," Agricultural and Forest Meteorology **101**, 237-246 (2000)

[28] J. Ross and V. Ross, "Statistical description of the architechture of a fast growing willow coppice," Agricultural and Forest Meteorology **91**, 23-37 (1998)

[29] G. G. Parker and M. E. Russ, "The canopy surface and stand development: assessing forest canopy structure and complexity with near-surface altimetry," Forest Ecology and Management **189**, 307-315 (2004)

[30] P. Meir, J. Grace, and A. C. Miranda, "Photographic method to measure the vertical distribution of leaf area density in forests," Agricultural and Forest Meteorology **102**, 105-111 (2000)

[31] H. S. Horn, "The adaptive geometry of trees, (Monographs in Population Biology)," Princeton University Press **9,** 144 (1971)

[32] Raymond Serway, *Physics for Scientists and Engineers with Modern Physics, 3rdEd,* Saunders College Publishing, (1990)

[33] F. Nicodemus, "Reflectance nomenclature and directional reflectance and emissivity," Appl. Opt., **9**, 1474-1475 (1970)

[34] T. W. Brakke, W. P. Wergin, E. F. Erbe, and J. M. Harnden, "Seasonal variation in the structure and red reflectance of leaves from Yellow Poplar, Red Oak, and Red Maple," Remote Sens. Environ. **43**, 115-130 (1993)

[35] Y. Wang and P. Jarvis, "Description and validation of an array model – MAESTRO," Agric. For Meteorol. **51**, 257-280 (1990)

[36] R. Pearcy and W. Yang, "A three-dimensional crown architecture model for assessment of light capture and carbon gain by understory plants," Oecologia **108**, 1-12 (1996)

[37] J. T. Woolley, "Reflectance and Transmittance of light by leaves," Plant Physiol. **47**, 656-662 (1972)

[38] http://en.wikipedia.org/wiki/Lambert%27s_cosine_law

[39] E. Vapaavouri, "Seasonal variation in the photosynthetic capacity of a willow (*Salix* cv. *Aquatica gigantea*) canopy," Tree Physiology **5**, 423-457 (1989)

[40] Kumar, R. "Radiation from Plants – Reflection and Emission: A Review," AA&ES **72-2-2**. Purdue University, Lafayette, Indiana (1972)

[41] Schilz, M. and Hurtt, G., "Factors Affecting the Pattern of Vegetation Biomass and Canopy Height With Elevation at Hubbard Brook Experimental Forest," American Geophysical Union, Fall Meeting (2005)

[42] http://en.wikipedia.org/wiki/Bidirectional_scattering_distribution_function

Appendices

Appendix A: Example: Approximation of Pi

For example, consider a circular dart board of radius r that is circumscribed by a square of length $2r$, as illustrated in Figure A.1. A Monte Carlo approximation to the value of pi can be performed by randomly "throwing" a number of darts at the circular dart board. Assume that (1) each dart lands in the square, and (2) the location of each dart is uniformly distributed on x and y. Then the ratio of the number of darts that land in the circle to the number of darts that land inside the square (all darts that land in the circle also land in the square) is approximately equal to the ratio of the areas of the circle and the square:

$$\frac{\pi r^2}{4r^2} = \frac{\pi}{4} \cong \frac{\#\text{ darts hitting in circle}}{\#\text{ darts hitting in square}} \tag{A.1}$$

Equation A.1 can be rearranged to give an approximation to the value of pi:

$$\pi \cong 4 \cdot \frac{\#\text{ darts hitting in circle}}{\#\text{ darts hitting in square}} \tag{A.2}$$

To begin, simulate the "throwing" of the first dart by selecting an x, y coordinate for the location of where the dart lands on the board. Assume that the thrower is blindfolded and therefore has an equal probability of throwing the dart anywhere on the board. The x and y locations of the dart are then described by two uniformly distributed

random variables which span the entire dart board and allow the dart to land anywhere on the board with equal probability. Let $x = y = 0$ be the center of the circle. Then, if $x^2 + y^2 \leq r$, the dart lands within the circle. Otherwise it lands outside the circle. Once the location of the first dart is confirmed, a second dart is "thrown" with a new random location on the board. As more and more darts are "thrown" one can begin to count the ratio of darts that land in the circle to those that land in the square and can approximate a value for pi.

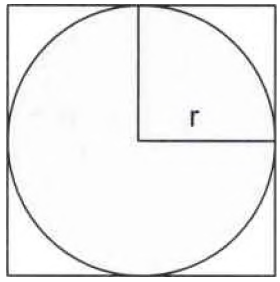

Figure A.1 A circular dart board of radius r is circumscribed by a square of side length $2r$.

The number of darts hitting inside the circle is a random quantity determined by the random locations of each of the darts. (Note that all the darts "thrown" land within the square.) Therefore, the calculated value of pi will vary for each simulation. Using Matlab, a Monte Carlo routine can be easily created to solve this simple problem. The Matlab algorithm described above involves selecting random x and y values for each dart. Whenever a dart lands within the circle, a counter index is increased. The value of the counter is divided into the total number of darts "thrown" and a value of pi is approximated.

The results of four separate simulations, each with a different number of realizations of darts thrown, N, are shown in Table A.1 below. Notice that here, as in all

Monte Carlo simulations, the calculated result is a random variable that differs from trial to trial. The only way to zero in on the actual value is to increase the number of realizations of the simulation, as stated by the law of large numbers. As the number of realizations increases, the accuracy of the simulation also increases.

Table A.1: Results of a Monte Carlo approximation of Pi

N	Calculated Pi	% Error
10	3.56	13.35
100	2.8	10.87
1000	3.088	1.70
10000	3.1468	0.165

This simple example illustrates the underlying concepts of simulating and approximating the solution of a system. The basic concept of creating a number of realizations and calculating the statistics of the outcome is a fundamental property of all Monte Carlo methods. The example above also illustrates that the Monte Carlo method for solving systems becomes an increasingly valid approximation as the number of realizations tends toward infinity.

Appendix B: Optical Path Lengths of Detector Channels

In order for the pulses of all the detectors to reach the oscilloscope at the same time, delay cables were attatched to the detectors to increase the optical path lengths of the detector channels by various amounts. The following are the measured optical path lengths from the front mirror of the laser to the respective detector heads for each channel.

Channel 1: Transmission

	Physical Length [inches]	medium
Laser → Beam Splitter	$10\frac{7}{16}$	air
Through BS	1	glass
BS → Target	$17\frac{6}{16}$	air
Target → Detector 1	$9\frac{15}{16}$	air

Total Optical Path Length $= 39\frac{2}{16}$ [in.]

Channel 2: Reflection

	Physical Length [inches]	medium
Laser → Beam Splitter	$10\frac{7}{16}$	air
Through BS	1	glass
BS → Target	$17\frac{6}{16}$	air
Target → Detector 2	$9\frac{15}{16}$	air

Total Optical Path Length $= 39\frac{2}{16}$ [in.]

Channel 3: Retro-Reflection

	Physical Length [inches]	medium
Laser → Beam Splitter	$10\frac{7}{16}$	air
Through BS	1	glass
BS → Target	$17\frac{6}{16}$	air
Target → BS	$17\frac{6}{16}$	air
Through BS	1	glass
BS → Mirror	$3\frac{4}{16}$	air
Mirror → Detector 3	$9\frac{14}{16}$	air

Total Optical Path Length $= 61\frac{5}{16}$ [in.]

Channel 4: Energy Monitor

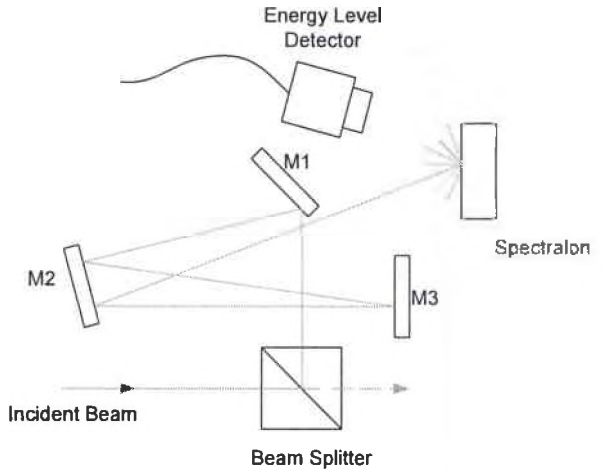

Figure B.1 Physical path of the beam en route to the energy level detector.

	Physical Length [inches]	medium
Laser → Beam Splitter	$10\frac{7}{16}$	air
Through BS	1	glass
BS → Mirror 1	$2\frac{4}{16}$	air
M1 → M2	$15\frac{1}{16}$	air
M2 → M3	$16\frac{2}{16}$	air
M3 → M2	$16\frac{2}{16}$	air
M2 → Spectralon	$17\frac{13}{16}$	air
Spectralon → Detector 4	$2\frac{11}{16}$	air

Total Optical Path Length = 82 [in.]

Appendix C: Derivation of Mean Projected Area

To begin the derivation of the mean projected area, suppose that the photon is incident from the $\hat{k}_0$ direction as illustrated in Figure C.1. That is, say that the observer is viewing from the $\hat{k}_0$ direction, which makes an angle of θ with the z-axis of the canopy. Also, assume that $\hat{k}_0$ lies in the x-y plane. This assumption is valid and should yield a general result since ϕ is uniform on the interval $[0,2\pi]$. Note, that because $\hat{k}_0$ does not have a y-dependence, it can be expressed as:

$$\hat{k}_0 = \hat{a}_x \sin\theta + \hat{a}_z \cos\theta . \tag{C.1}$$

The leaf angle orientation is described by the leaf normal vector $\hat{a}_N$ which is defined by the leaf zenith θ_l and azimuth ϕ_l angles to be:

$$\hat{a}_N = \hat{a}_x \sin\theta_l \cos\phi_l + \hat{a}_y \sin\theta_l \sin\phi_l + \hat{a}_z \cos\phi_l . \tag{C.2}$$

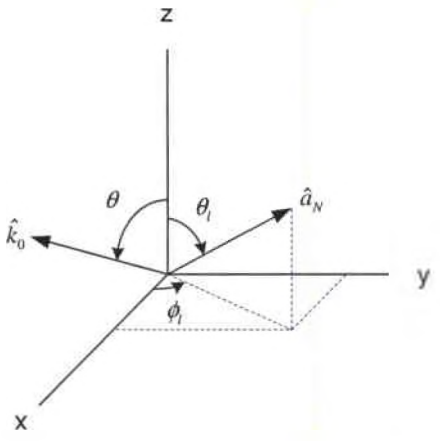

Figure C.1 Angular orientation of illumination direction $\hat{k}_0$ and leaf surface normal $\hat{a}_N$

The projected area is found by projecting the generalized ray propagation vector onto the generalized leaf area vector. This is achieved by applying the dot product to the two vectors, which gives the projected area to be

$$A_p = A_0 \hat{a}_N \cdot \hat{k}_o . \tag{C.3}$$

Rewriting these two vectors in terms of the angles that define them yields the expression,

$$A_p = \frac{\pi d^2}{4}\left[\hat{a}_x \sin\theta_l \cos\phi_l + \hat{a}_y \sin\theta_l \sin\phi_l + \hat{a}_z \cos\phi_l\right]\cdot\left[\hat{a}_x \sin\theta + \hat{a}_z \cos\theta\right]$$

which is solved to give:

$$A_p = \frac{\pi d^2}{4}\left[\sin\theta_l \cos\phi_l \sin\theta + \cos\phi_l \cos\theta\right] \tag{C.4}$$

The next step is to average this projected area over all possible orientations of the leaf. Intergration over the two leaf orientation angles will arrive at the mean projected leaf area. Recall that the leaf orientation angles are each governed by their own probability density function, which must be taken into the integral with the projected area. Applying these functions yields the expression for the mean projected area,

$$\overline{A}_p = \frac{2}{2\pi}\int_0^{\frac{\pi}{2}}\int_{-\frac{\pi}{2}}^{\frac{\pi}{2}} A_p \cos\theta_l d\phi_l d\theta_l \tag{C.5}$$

Caution must be taken when applying the boundaries of the integration. Area vectors possess both magnitude and direction, and therefore negative areas are a possibility. If the top side area of the leaf is defined to be positive then the underside area of the leaf must be negative. This causes trouble when the leaf is examined over the entire range of the azimuth angles. The negative area found when observing the leaf's underside subtracts to cancel out the positive area when observing the leaf's top side. Because the model is indiscriminant of which side of the leaf is hit, instead of integrating

ϕ over the range $[0,2\pi]$, integrate over $\left[-\frac{\pi}{2},\frac{\pi}{2}\right]$ and multiply the result by 2 to account for both the top and bottom sides of the leaf.

Substitute in the expression for A_p found in Equation C.5 and perform the integration.

$$\bar{A}_p = \frac{\pi d^2}{4}\frac{2}{2\pi}\int_0^{\frac{\pi}{2}}\int_{-\frac{\pi}{2}}^{\frac{\pi}{2}}\left[\sin\theta_l\cos\phi_l\sin\theta+\cos\theta_l\cos\theta\right]\cos\theta_l d\phi_l d\theta_l \tag{C.6}$$

Distribute $\cos\theta_l$ through the integral.

$$\bar{A}_p = \frac{d^2}{4}\int_0^{\frac{\pi}{2}}\int_{-\frac{\pi}{2}}^{\frac{\pi}{2}}\sin\theta_l\cos\phi_l\sin\theta\cos\theta_l+\cos^2\theta_l\cos\theta d\phi_l d\theta_l \tag{C.7}$$

Integrating over ϕ_l gives

$$\begin{aligned}\bar{A}_p &= \frac{d^2}{4}\int_0^{\frac{\pi}{2}}\sin\theta_l\sin\theta\cos\theta_l\sin\phi_l\Big|_{-\frac{\pi}{2}}^{\frac{\pi}{2}}+\cos^2\theta_l\cos\theta\phi_l\Big|_{-\frac{\pi}{2}}^{\frac{\pi}{2}}d\theta_l \\ &= \frac{d^2}{4}\int_0^{\frac{\pi}{2}}\sin\theta_l\sin\theta\cos\theta_l(1-(-1))+\cos^2\theta_l\cos\theta\left(\frac{\pi}{2}-\left(-\frac{\pi}{2}\right)\right)d\theta_l\end{aligned}$$

$$\bar{A}_p = \frac{d^2}{4}\int_0^{\frac{\pi}{2}}2\sin\theta_l\cos\theta_l\sin\theta+\pi\cos^2\theta_l\cos\theta d\theta_l \tag{C.8}$$

Perform the following substitutions onto the first and second terms of the integrand. On the first term, make the substitution, $u=\sin\theta_l$ and $du=\cos\theta_l d\theta_l$. On the second term, use the trig identity, $\cos^2\theta_l=\frac{1}{2}(1+\cos 2\theta_l)$. Applying these substitutions and integrating yields,

$$\bar{A}_p = \frac{d^2}{4}\left[2\frac{1}{2}\sin^2\theta_l\Big|_0^{\frac{\pi}{2}}\sin\theta+\pi\cos\theta\frac{1}{2}\int_0^{\frac{\pi}{2}}1+\cos 2\theta_l\, d\theta_l\right] \tag{C.9}$$

Evaluating the result at the boundary conditions gives

$$\overline{A}_p = \frac{d^2}{4}\left[\sin\theta + \pi\cos\theta\frac{1}{2}\left(\frac{\pi}{2} + \frac{1}{2}\sin 2\theta_l\Big|_0^{\frac{\pi}{2}}\right)\right] \tag{C.10}$$

$$\overline{A}_p = \frac{d^2}{4}\left[\sin\theta + \pi\cos\theta\left(\frac{\pi}{4} + \frac{1}{4}(0-0)\right)\right] \tag{C.11}$$

Finally, a final expression for the mean projected area is found.

$$\overline{A}_p(\theta) = \frac{d^2}{4}\left[\sin\theta + \frac{\pi^2}{4}\cos\theta\right] \tag{C.12}$$

Appendix D: Differentiation of Leaf Area Density Function

Since the derivative of the LAD describes the slope of the tangent to the LAD curve, higher values of the derivative correspond to regions of great change in the LAD curve. Similarly, smaller values of the derivative correspond to areas where the LAD function remains relatively constant. Recall that the expression for the leaf area density as a function of canopy height is given by Equation D.1, where $z = 0$ refers to the top of the canopy (sky), and $z = T$ refers to the bottom (ground). Begin taking the derivative of this function by pulling out the constants:

$$\begin{aligned} \frac{d}{dz}L(z) &= \frac{d}{dz}\left[L_m \left(\frac{z_m}{z}\right)^n \exp\left(n\left(1-\frac{z_m}{z}\right)\right)\right] \\ &= L_m z_m{}^n \frac{d}{dz}\left[z^{-n} \exp\left(n\left(1-\frac{z_m}{z}\right)\right)\right] \end{aligned} \tag{D.1}$$

The derivative of this expression can be performed by using the product rule of differentiation,

$$\begin{aligned} \frac{d}{dz}L(z) &= L_m z_m{}^n \left[\exp\left(n\left(1-\frac{z_m}{z}\right)\right)\frac{d}{dz}\left[z^{-n}\right] + z^{-n}\frac{d}{dz}\left[\exp\left(n\left(1-\frac{z_m}{z}\right)\right)\right]\right] \\ &= L_m z_m{}^n \left[\left[-nz^{-(n+1)}\right]\exp\left(n\left(1-\frac{z_m}{z}\right)\right) + \left[\frac{nz_m}{z^2}\exp\left(n\left(1-\frac{z_m}{z}\right)\right)\right] z^{-n}\right] \\ &= L_m z_m{}^n \left[\left[-nz^{-(n+1)}\right]\exp\left(n\left(1-\frac{z_m}{z}\right)\right) + \left[nz_m z^{-(n+2)}\exp\left(n\left(1-\frac{z_m}{z}\right)\right)\right]\right] \end{aligned}$$

Which gives,

$$\frac{d}{dz}L(z) = L_m z_m{}^n n \exp\left(n\left(1-\frac{z_m}{z}\right)\right) z^{-n}\left[z^{-1} + z_m z^{-2}\right] \tag{D.2}$$

Simplifying this expression yields the function for the change in leaf area density as a function of canopy height:

$$\frac{d}{dz}L(z) = L_m\left(\frac{z_m}{z}\right)^n n\left[z^{-1} + z_m z^{-2}\right]\exp\left(n\left(1-\frac{z_m}{z}\right)\right) \tag{D.3}$$

What is important here is the magnitude of the derivative. Whether the dLAD function is positive or negative is not an issue, just the magnitude of the change in LAD. So the absolute value of the derivative of the leaf area density function is what is interesting. The shape of the absolute value of the dLAD function (blue) compared to the shape of the LAD curve (red) is shown in Figure D.1. Notice that the maximum value of the dLAD curve occurs when the LAD function experiences the greatest amount of change.

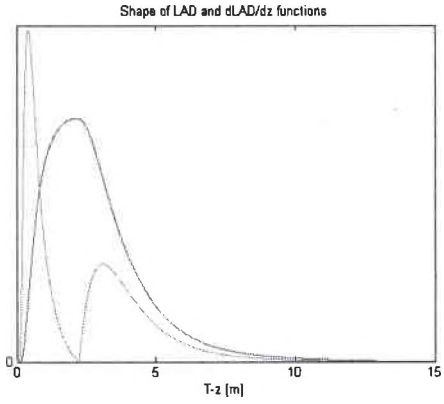

Figure D.1 Shape of the leaf area density function (blue) and its derivative (red) as a function of canopy height

Appendix E: Illumination Angle Calculation

In the case where the BRDF of leaves is modeled as both a diffuse component and a specular component, the angle of incidence of the photon onto the leaf is a critical measurement. Whereas when perfect Lambertian distribution is assumed, the angle of incidence of the photon is irrelevant because the scattering profile is cosinusoidal regardless of illumination angle. It is therefore necessary to calculate the angle made between the incident photon and the surface normal of the leaf.

Recall that the leaf angles are given in the canopy coordinate system as θ_L and ϕ_L. We can also describe the orientation of the incident photon by using the spatial locations of the photon at the current $(X(j), Y(j), Z(j))$ and previous $(X(j-1), Y(j-1), Z(j-1))$ locations. A vector analysis of these known variables allows us to calculate the angle made between the leaf and the incident photon. The ray vector $\bar{r}$, which gives the propagation direction of the photon, is given to be:

$$\bar{r} = [X(j) - X(j-1), Y(j) - Y(j-1), Z(j) - Z(j-1)] \tag{E.1}$$

Let $Q(1) = X(j) - X(j-1)$, $Q(2) = Y(j) - Y(j-1)$, and $Q(3) = Z(j) - Z(j-1)$.

Then,

$$\bar{r} = [Q(1), Q(2), Q(3)] \tag{E.2}$$

The leaf normal vector $\bar{l}$ is given by

$$\bar{l} = [\sin\theta_L \cos\phi_L, \sin\theta_L \sin\phi_L, \cos\theta_L]. \tag{E.3}$$

The dot product of two vectors relates the magnitudes of the vectors and the angle between the vectors to the projection of one vector onto the other. Let $\bar{v}$ and $\bar{w}$ be any two vectors, and let α be the angle separating the two, then

$$\vec{v} \bullet \vec{w} = |\vec{v}||\vec{w}| \cos \alpha . \tag{E.4}$$

So,

$$\vec{r} \bullet \vec{l} = Q(1) \sin \theta_L \cos \phi_L + Q(2) \sin \theta_L \sin \phi_L + Q(3) \cos \theta_L \tag{E.5}$$

Also, if $d(j)$ is the distance traveled by the photon during the propagation of the ray vector, then

$$|\vec{r}||\vec{l}| = d(j) \cdot 1 \tag{E.6}$$

Therefore, the angle between the incident photon and the leaf normal is given by

$$\theta_l = \cos^{-1} \left[\frac{Q(1) \sin \theta_L \cos \phi_L + Q(2) \sin \theta_L \sin \phi_L + Q(3) \cos \theta_L}{d(j)} \right] \tag{E.7}$$

This angle allows us to known which BRDF to use during the random scattering angle selection phase of the code. Because of the specular reflection component, it is important to know at exactly what angle the leaf is struck.

Appendix F: Coordinate Transformation

Once the scattering angles have been selected from the leaf, it is necessary to transform the angles from the coordinate system of the leaf to the coordinate system of the canopy in order to track the spatial locations of the photons. Figure F.1 displays the angular orientation for the zenith and azimuth scattering angle. The axes in the figure are the coordinate axes of the leaf with the leaf normal being the z'-axis. This coordinate system must be transformed back to the coordinate system of the canopy, where the z-axis points directly downwards.

The first step in transforming the coordinate systems is to create a unit vector in the direction of the scattered photon in the coordinate system of the leaf normal. The unit vector representing the direction of the scattered photon is given by,

$$[xs, ys, zs] = [\sin\theta_S \cos\phi_S, \sin\theta_S \sin\phi_S, \cos\theta_S] \tag{F.1}$$

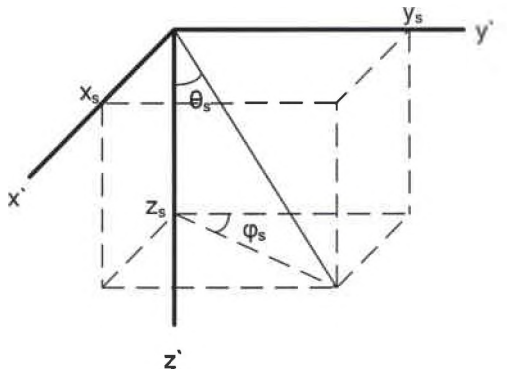

Figure F.1 Angular orientations for scattering from a leaf

The unit scattering vector is then transformed by a simple transformation matrix. The transformation consists of two individual rotations: (1) rotation of angle ϕ_L about the

z-axis, and (2) rotation of angle θ_L about the y-axis. The first transformation has a transformation matrix given by

$$M_1 = \begin{bmatrix} \cos\phi_L & -\sin\phi_L & 0 \\ \sin\phi_L & \cos\phi_L & 0 \\ 0 & 0 & 1 \end{bmatrix}. \tag{F.2}$$

The second rotation has a transformation matrix given by

$$M_2 = \begin{bmatrix} \cos\theta_L & 0 & \sin\theta_L \\ 0 & 1 & 0 \\ -\sin\theta_L & 0 & \cos\theta_L \end{bmatrix} \tag{F.3}$$

The transformations are combined by multiplying the individual transformation matrices together. Note that when combining transformations, the order in which they are performed (as if done separately) is M_2 then M_1, then $M = M_1 M_2$, if M is the combined transformation. So,

$$M = \begin{bmatrix} \cos\phi_L & -\sin\phi_L & 0 \\ \sin\phi_L & \cos\phi_L & 0 \\ 0 & 0 & 1 \end{bmatrix} \cdot \begin{bmatrix} \cos\theta_L & 0 & \sin\theta_L \\ 0 & 1 & 0 \\ -\sin\theta_L & 0 & \cos\theta_L \end{bmatrix} \tag{F.4}$$

$$M = \begin{bmatrix} \cos\theta_L\cos\phi_L & -\sin\phi_L & \sin\theta_L\cos\phi_L \\ \cos\theta_L\sin\phi_L & \cos\phi_L & \sin\theta_L\sin\phi_L \\ -\sin\theta_L & 0 & \cos\theta_L \end{bmatrix} \tag{F.5}$$

Once the transformation matrix is calculated for the leaf orientation, multiplication of the unit scattering vector by this transformation matrix allows the calculation of the new propagation angles of the photon in the coordinate system of the canopy. The vector describing the propagation distance of the unit vector (leaf coordinate system) in the canopy coordinate system is shown in Figure F.2, and given by

$$W = [W(1), W(2), W(3)] = M[xs; yx; zs]. \tag{F.6}$$

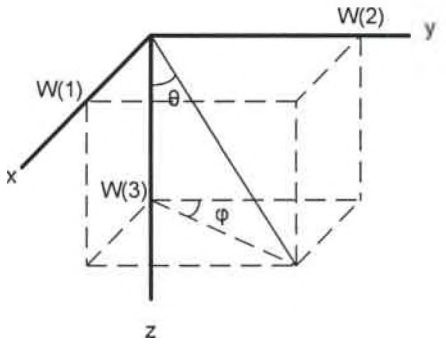

Figure F.2 Relative axis scattering distances

The actual scattering angles from the leaf in the canopy coordinate system are then given by the inverse trig functions of the W-vector:

$$\theta(j) = \tan^{-1}\left(\frac{\sqrt{W(1)^2 + W(2)^2}}{W(3)}\right) \tag{F.7}$$

$$\phi(j) = \tan^{-1}\left(\frac{W(2)}{W(1)}\right) \tag{F.8}$$

Now we have the random scattering angles from the randomly oriented leaf in the coordinate system of the canopy. This is the new propagation direction of the photon.

Appendix G: Backwards Ray Tracing for Side Scattering

For the case where a photon is side scattered from the canopy, the final location of the photon lies outside the canopy. We need to trace the path of the photon back to the edge of the canopy. The previous location of the last leaf interaction and the angular direction of travel of the photon are known.

Beginning from the previous location of the photon and using the known propagation direction of the photon, we want to find the exact location where the photon exits the canopy. We know that the radius of the photon upon exit is the radius of the canopy, which is given by R. To begin, assume that the distance traveled from the previous location to the edge of the canopy is D. Then, by geometry, the distance that the photon traveled in the x-direction before exiting the canopy is given by $D\sin\theta\cos\phi$. Similarly, the distance traveled in the y-direction is given by $D\sin\theta\sin\phi$.

So, the x-location of the photon at the edge of the canopy is given by the expression

$$X(j) = X(j-1) + D\sin\theta\cos\phi \tag{G.1}$$

and the y-location of the photon at the edge of the canopy is then given by

$$Y(j) = Y(j-1) + D\sin\theta\sin\phi\ . \tag{G.2}$$

The problem now is to solve for D and find the distance traveled by the photon to the edge of the canopy. We know that

$$R = \sqrt{X(j)^2 + Y(j)^2}\ .$$

Substituting in the expressions A7.1 and A7.2 gives

$$R = \sqrt{(X(j-1) + D\sin\theta\cos\phi)^2 + (Y(j-1) + D\sin\theta\sin\phi)^2} \tag{G.3}$$

Squaring both sides of the equation and expanding the right side yields

$$\begin{aligned} R^2 &= X^2 + 2XD\sin\theta\cos\phi + D^2\sin^2\theta\cos^2\phi \\ &\quad + Y^2 + 2YD\sin\theta\sin\phi + D^2\sin^2\theta\sin^2\phi \end{aligned} \tag{G.4}$$

Collecting the terms into powers of D gives

$$\begin{aligned} 0 &= \left(X^2 + Y^2 - R^2\right) + D(2X\sin\theta\cos\phi + 2Y\sin\theta\sin\phi) \\ &\quad + D^2\left(\sin^2\theta\cos^2\phi + \sin^2\theta\sin^2\phi\right) \end{aligned} \tag{G.5}$$

Solve this expression for D using the quadratic formula.

$$D = \frac{-b \pm \sqrt{b^2 - 4ac}}{2a} \tag{G.6}$$

Where, $a = \left(X^2 + Y^2 - R^2\right)$, $b = (2X\sin\theta\cos\phi + 2Y\sin\theta\sin\phi)$, and

$c = \left(\sin^2\theta\cos^2\phi + \sin^2\theta\sin^2\phi\right)$.

Now that the distance traveled to the edge of the canopy is known, the spatial and temporal locations of the photon at the canopy's edge can be calculated:

$$X(j) = X(j-1) + D\sin\theta\cos\phi$$

$$Y(j) = Y(j-1) + D\sin\theta\sin\phi$$

$$Z(j) = Z(j-1) + D\cos\theta$$

$$d(j) = D$$